Spin and quadrupolar effects in the secular evolution of precessing compact binaries with black hole, neutron star, gravastar, or boson star components

Zoltán Keresztes,[*] Márton Tápai,[†] and László Árpád Gergely[‡]
Institute of Physics, University of Szeged, Dóm tér 9, Szeged 6720, Hungary

(Received 7 August 2020; accepted 8 January 2021; published 13 April 2021)

We discuss precessing compact binaries on eccentric orbit with gravastar, black hole, neutron star, or boson star components. We derive the secular evolution equations to second post-Newtonian–order accuracy, with leading-order spin-orbit, spin-spin, and mass quadrupole-monopole contributions included. The emerging closed system of first-order differential equations evolves the pairs of polar and azimuthal angles of the spin and orbital angular momentum vectors together with the periastron angle. In contrast with the instantaneous dynamics, the secular dynamics is autonomous. The validity of the latter is confirmed numerically, showing that secular evolutions look like smoothed-out instantaneous evolutions over timescales where radiation reaction is negligible. The secular evolution of the spin polar angles and the difference of their azimuthal angles generates a closed subsystem, which, despite the apparent singularity of spherical polar coordinates, remains well defined through aligned configurations. We study analytically this system for the particular cases of one spin dominating over the other and for black hole - boson star binaries of equal masses. In the first case, known large flip-flops of the smaller spin are reproduced, when the larger spin is almost coplanar with the orbit. We also find new, quadrupole-induced flip-flops occurring when the neutron star with dominant spin has a quadrupolar parameter $w_1 \approx 3$. Finally, we analyze the evolutions of the spin angles numerically by comparing the cases when the black hole companion is either a gravastar, another black hole, or a boson star with identical mass. We find that both the amplitude and period of the flip-flop are the largest, when the companion is a black hole. In the case of a boson star companion, the frequency of the flip-flop increases significantly. Further, while in the case of gravastars and black holes a swinging-type azimuthal evolution occurs, with the spins of the components periodically overpassing each other, their sequence is conserved when the companion is a boson star.

DOI: 10.1103/PhysRevD.103.084024

I. INTRODUCTION

In the O1 and O2 runs of the Advanced LIGO Detector, the LIGO Scientific Collaboration and the Virgo Collaboration have announced a total of 11 gravitational wave detections, ten of them produced by coalescing stellar mass black holes [1], while in one case, the source was a coalescing neutron star binary [2]. A much larger event rate has been seen in the more sensitive O3 run, with 39 compact binary mergers identified during its first half [3], among them other plausible neutron star mergers and neutron star - black hole mergers. The spin of the merging black holes was identified with high significance in two cases during the O1–O2 runs [1,4], while in the first half of the O3 run, nine events were identified with the effective spin parameter nonvanishing in the 90% symmetric credible interval [3]. The accurate description of both the orbital and spin dynamics of compact binary systems is important for gravitational wave source modeling; however, the imprint of spin effects also occurs in radio astronomy. From the analysis of Very Long Baseline Interferometry (VLBI) radio data of a binary spanning over 18 years, the spin precession of the dominant supermassive black hole could be identified [5].

Whenever the black hole spins $\mathbf{S_1}$, $\mathbf{S_2}$, and the Newtonian orbital angular momentum $\mathbf{L_N}$ of the binary are not aligned, they undergo precession [6–8]. The total angular momentum $\mathbf{J} = \mathbf{L} + \mathbf{S_1} + \mathbf{S_2}$ composed of the total orbital angular momentum $\mathbf{L}$ and the individual spins is conserved up to the second post-Newtonian (2PN) order [9–12], radiative dissipation appearing at 2.5PN orders [13]. Both conservative and dissipative contributions to dynamics arising from leading 1.5PN-order spin-orbit (SO) coupling have been thoroughly analyzed [14,15], as were the 2PN spin-spin (SS) [16–18] and the 2PN mass quadrupole-mass monopole (QM) contributions [19–24]. The 2PN self-interaction spin effect in the radiative losses, representing the 2PN correction to the 1.5PN-order Lense-Thirring approximation, was first identified in Refs. [16,17] and explored later to derive the respective contributions to the

[*]zkeresztes@titan.physx.u-szeged.hu
[†]tapai@titan.physx.u-szeged.hu
[‡]gergely@physx.u-szeged.hu

accumulated orbital phase [25]. The dynamics of compact binary systems has been analyzed to 4PN-order accuracy either in the nonspinning case [26,27], or in a conservative approach at the Hamiltonian level [28]. Hamiltonian methods applied for compact binaries generated several notable results; see Ref. [29] and references herein.

Compact binary dynamics in the inspiral regime exhibit three distinct timescales. The shortest is the radial timescale, defined by the period of the orbital motion of the reduced mass. Under the precessional timescale, the orbital angular momentum $\mathbf{L_N}$ and the spins $\mathbf{S_1}$ and $\mathbf{S_2}$ undergo a full rotation about their precession axis. Over the gravitational radiation reaction timescale, the effects of gravitational dissipation become noticeable. Averaging the dynamics over any of these timescales may be rewarding. When precession-related effects are targeted, averaging over a radial period will remove insignificant instantaneous effects but keep the dominant precessional evolution. Several interesting spin-related evolutions were identified by this method. When the orbital angular momentum nearly cancels the total spin, the orbital plane changes significantly during a relatively short-lived transitional precession period [30]. The direction of dominant spin relative to the total angular momentum can change significantly over the radiation reaction timescale in binaries where the components have significantly different mass [31]. This spin flip may explain the formation of X-shape radio galaxies [32]. By an additional averaging over the precession timescale, the evolution of the magnitude of total angular momentum over the radiation reaction timescale was investigated in Refs. [33,34].

When the dominant spin vector is approximately perpendicular to $\mathbf{L_N}$ and the smaller spin is closely aligned with it, the smaller spin slowly evolves to be antialigned with $\mathbf{L_N}$, then periodically changes back and forth on a timescale shorter than the gravitational radiation reaction timescale [35]. This effect was investigated in a wider parameter range for binaries moving on circular orbits [36,37]. This spin flip-flop effect was first found qualitatively in Ref. [38] as a harmonic "wooble" in the polar angle of the spin, which evolves "from pole to pole." Recently, a parameter range has been identified where the flip-flop happens on relatively short timescales, dubbed as wide precession [39]. Then, over the period during which the magnitude of the total spin changes from its minimum to its maximum and back to the minimum value, one of the two spins evolves from complete alignment with $\mathbf{L_N}$ to complete antialignment.

Kidder has derived the orbit-averaged (secular) spin-precession equations [10] for circular orbits, with SO and SS contributions included, but QM contributions omitted. The QM couplings were included in the discussion of angular evolutions in black hole binaries (where the quadrupole parameters are $w_i = 1$) by Racine [21], who presented a new constant of motion λ of the orbit-averaged dynamics (or equivalently $\xi = \lambda L_N$, the last factor representing the magnitude of $\mathbf{L_N}$).

Racine also solved analytically the averaged equations for equal masses and derived approximate analytical solutions in the unequal mass case. His analytical solution has been generalized for arbitrary masses and spins (but still $w_i = 1$ and circular orbits) in Ref. [40], which identified three distinct regimes in the orbit-averaged precessional dynamics: librations about the configurations of the two spin projections to the orbital plane either aligned or antialigned and a "circulating" configuration, when one of the spins precesses much faster.

Because of the recent discovery of gravitational waves from mergers of neutron stars [2,41], the interest in their internal structure and equation of state [42], implying a better constrained range of the parameter w_i, has been revitalized. In this work, we leave the quadrupole parameter unspecified, including neutrons stars with $w_i \in (2,14)$ [43,44] and also other exotic compact objects, like boson stars with $w_i \in (10, 150)$ [45] or gravastars with $w_i \in (-0.8, 1)$ [46] as compact binary components. Allowing for $w_i \neq 1$ complicates the dynamics, as for example, the quantity conserved for black hole binaries, identified by Racine, becomes dynamical, unless $w_i = 1$.

Although gravitational radiation tends to circularize the orbit of the binary [13], significant eccentricity can be preserved at the end of the inspiral. This happens for binaries in either dense galactic nuclei [47,48] or within accretion disks [49,50]. Furthermore, because of the Kozai mechanism, the relativistic orbital resonances in hierarchical triples can also retain eccentricity [51–54]. The interaction between supermassive black hole binaries and their star populations results in significant eccentricity toward the end of the inspiral, too [55,56]. Hence, allowing for eccentricity in the dynamics may be rewarding.

The instantaneous dynamics (including SO, SS, and QM effects, also eccentricity) in terms of dimensionless variables was discussed in Refs. [57–59], based on earlier works on binary dynamics of Refs. [6–9,60–63]. The 2PN conservative dynamics of compact binary systems was given by Eqs. (36)–(42) of Ref. [59] in terms of dimensionless osculating orbital elements $\mathfrak{l}_r$, e_r, ψ_p, α, and ϕ_n; spin polar and azimuthal angles κ_i and ζ_i ($i = 1, 2$); and true anomaly parameter χ_p. The time evolution of χ_p is governed by Eq. (43) of Ref. [59]. The polar angles κ_i of the spin vectors are measured from $\mathbf{L_N}$. The azimuthal angles ζ_i are measured from the Laplace-Runge-Lenz vector $\mathbf{A_N}$ in the plane perpendicular to $\mathbf{L_N}$. The argument of the periastron, ψ_p is defined by $\psi_p = \arccos(\hat{\mathbf{l}} \cdot \hat{\mathbf{A}}_\mathbf{N})$, with $\hat{\mathbf{l}} = \hat{\mathbf{J}} \times \hat{\mathbf{L}}_\mathbf{N}$, where $\hat{\mathbf{J}}$ is the direction of the total angular momentum, which is conserved in the 2PN dynamics. The inclination α is the polar angle of $\hat{\mathbf{L}}_\mathbf{N}$ measured from $\hat{\mathbf{J}}$. The last angle is the longitude of the ascending node $-\phi_n$, spanned by the inertial axis $\hat{\mathbf{x}}$ (arbitrarily chosen in the plane perpendicular to $\hat{\mathbf{J}}$) and $\hat{\mathbf{l}}$. This angle is related to the azimuthal angle $(\pi/2 - \phi_n)$ of $\hat{\mathbf{L}}_\mathbf{N}$, measured from $\hat{\mathbf{x}}$ in the

plane perpendicular to $\hat{\mathbf{J}}$. (The angles χ_p, κ_i, $\psi_i = \zeta_i - \psi_p$, ψ_p, α, and ϕ_n are shown in Fig. 2 in Ref. [57].)

The dimensionless orbital angular momentum

$$\mathfrak{l}_r = \frac{cL_N}{Gm\mu} \tag{1}$$

and the eccentricity

$$e_r = \frac{A_N}{Gm\mu} \tag{2}$$

characterize the osculating ellipse of the orbit; hence, they are shape variables. The total and reduced masses of the binary are denoted as $m = m_1 + m_2$ and $\mu = m_1 m_2/m$, respectively. We also employ the mass ratio $\nu = m_2/m_1 \leq 1$ and the symmetric mass ratio $\eta = \mu/m$. The gravitational constant, the speed of light, and the magnitude of $\mathbf{A_N}$ are denoted by G, c, and A_N, respectively. The magnitudes of the spins are characterized by the dimensionless spin parameters $\chi_i = cS_i/Gm_i^2$ $(i = 1, 2)$. The dot will denote the derivative with respect to the dimensionless time variable $\mathfrak{t} = tc^3/Gm$ (with time t) introduced in Ref. [59]. The PN parameter is defined as $\varepsilon = Gm/c^2 r$.

In this paper, we will investigate precessing compact binary systems on eccentric orbit subject to bound motion, first establishing the 2PN secular dynamics in terms of the above-mentioned dimensionless variables, then analyzing the spin evolutions with the methods of dynamical systems, with SO, SS, and QM contributions included. The PN equations of motion depend on the choice of a spin supplementary condition (SSC).[1] We employ the Newton-Wigner-Price [65,66] SSC, similarly as in Ref. [59]. This system is valid for eccentric orbits and for binaries composed of either black holes, neutron stars, or other exotic compact objects (boson stars or gravastars).

The instantaneous dynamics described in Ref. [59] is averaged over a suitably defined radial period in Sec. II, obtaining the secular precessing compact binary dynamics in terms of the dimensionless osculating orbital elements $\mathfrak{l}_r$, e_r, ψ_p, α, ϕ_n, and spin angles κ_i, ζ_i $(i = 1, 2)$. These equations contain PN, SO, SS, QM, and 2PN contributions. These are generalized Lagrangian planetary equations, which become singular for vanishing e_r; nevertheless, the singularity can be eliminated by a transformation of variables [67]. For completeness, we also give in this section the secular precession angular velocities and constraints relating the variables.

For the purpose of averaging, the PN expansion of the radial period is required. For clarity of presentation, we deferred the tedious but straightforward bulk of calculations leading to it to the lengthy Appendix A. There, first, we derive the radial period in terms of the variables evaluated at the periastron (characterized by the value of the true anomaly parameter $\chi_p = 0$). The χ_p dependence of the shape variables is also derived by integrating the corresponding first-order system given in Ref. [59]. Then, we compute their time-averaged values $\bar{\mathfrak{l}}_r$, $\bar{e}_r$ over the radial period to 2PN accuracy, with the inclusion of all spin and mass quadrupole effects to this order. Next, we express the shape variables evaluated in the periastron in terms of the corresponding averaged quantities. With this, we can write the radial period as a PN expansion expressed in terms of averaged quantities. We also give there a similar expansion in terms of the chosen variables of the PN parameter.

In Sec. III, we analyze the role of eccentricity in the secular evolution by comparing low-eccentricity and medium-eccentricity evolutions for the values of the PN parameter 0.01 and 0.0005. We also prove that the secular dynamics follows closely the instantaneous dynamics given in Ref. [59] over the conservative timescale.

The secular evolution of the spin angles generates a closed subsystem of three variables, discussed in Sec. IV. Despite the apparent singularity of spherical polar coordinates, we prove in Appendix B that the system remains well defined through aligned configurations.

In Sec. V, we study analytically and numerically this closed subsystem for the particular case of one spin dominating over the other, concentrating on the flip-flop effect of the polar angle of the smaller spin. We identify a diamond-shaped region in the parameter plane span by the dominant spin polar angle and quadrupolar parameter. Along the horizontal axis of the diamond, the known flip-flop effect for black hole binaries is reproduced; however, the vertical axis signifies mass quadrupole-induced flip-flops occurring for neutron stars with a particular quadrupolar parameter.

In Sec. VI, we study the closed subsystem for the particular case of black hole - boson star binaries. We investigate the spin angle dynamics both analytically and numerically. We also compare it to typical evolutions in black hole - black hole and black hole - gravastar binaries, pointing out the differences.

In Sec. VII, we present the conclusions.

II. SECULAR CONSERVATIVE DYNAMICS OF PRECESSING COMPACT BINARIES

In this section, we present the orbital averaged evolution equations of the dimensionless osculating orbital elements $\mathfrak{l}_r$, e_r, ψ_p, α, and ϕ_n and spin angles κ_i, ζ_i $(i = 1, 2)$ at 2PN accuracy, with spin and mass quadrupole effects included from the instantaneous evolutions derived in Ref. [59].

[1]A comparison of the three widely used SSCs has been presented in Ref. [64], proving the SSC dependence of the radiative multipole moments.

A. Averaging method

For bounded motion, the separation r between the binary components can be parametrized similarly to a Keplerian orbit [59],

$$\frac{c^2 r}{Gm} = \frac{\mathfrak{l}_r^2}{1 + e_r \cos\chi_p}, \tag{3}$$

where χ_p is the true anomaly. However, unlike a Keplerian orbit, both shape variables $\mathfrak{l}_r$ and e_r are time dependent.

The dimensionless period $\mathfrak{T}$ is defined as the change in the dimensionless time $\mathfrak{t} \equiv tc^3/Gm$ during the evolution of the true anomaly over $\chi_p \in [0, 2\pi]$ as

$$\mathfrak{T} \equiv \int_0^{\mathfrak{T}} d\mathfrak{t} = \int_0^{2\pi} \frac{d\chi_p}{\dot{\chi}_p}. \tag{4}$$

The average $\bar{f}$ of any quantity $f(\mathfrak{t})$ with respect to $\mathfrak{t}$ is introduced by

$$\mathfrak{T}\bar{f} = \int_0^{\mathfrak{T}} f(\mathfrak{t}) d\mathfrak{t} = \int_0^{2\pi} \frac{f(\chi_p)}{\dot{\chi}_p} d\chi_p. \tag{5}$$

Then, as described in Appendix A, the period can be rewritten in terms of the orbital averaged shape variables as

$$\mathfrak{T} = \tilde{\mathfrak{T}}\left(1 + \frac{1}{\bar{\mathfrak{l}}_r^2}\tilde{\tau}_{PN} + \frac{1}{\bar{\mathfrak{l}}_r^3}\tilde{\tau}_{SO} + \frac{1}{\bar{\mathfrak{l}}_r^4}\tilde{\tau}_{QM} + \frac{1}{\bar{\mathfrak{l}}_r^4}\tilde{\tau}_{SS} + \frac{1}{\bar{\mathfrak{l}}_r^4}\tilde{\tau}_{2PN}\right), \tag{6}$$

with the expressions $\tilde{\mathfrak{T}}$, $\tilde{\tau}_{PN}, \tilde{\tau}_{SO}, \tilde{\tau}_{QM}, \tilde{\tau}_{SS}$, and $\tilde{\tau}_{2PN}$ also given there. Here, $1/\mathfrak{l}_r^2$ stands for one relative PN order, as indicated by Eq. (8) of Ref. [59].

B. Shape variables

Employing the averaging method described in the previous section, long but straightforward calculations lead to the secular evolutions of the dimensionless orbital angular momentum $\mathfrak{l}_r$ and orbital eccentricity e_r as

$$\bar{\dot{\mathfrak{l}}}_r = \bar{\dot{\mathfrak{l}}}_r^{PN} = \bar{\dot{\mathfrak{l}}}_r^{SO} = \bar{\dot{\mathfrak{l}}}_r^{SS} = \bar{\dot{\mathfrak{l}}}_r^{QM} = \bar{\dot{\mathfrak{l}}}_r^{2PN} = 0, \tag{7}$$

$$\bar{\dot{e}}_r = \bar{\dot{e}}_r^{PN} = \bar{\dot{e}}_r^{SO} = \bar{\dot{e}}_r^{SS} = \bar{\dot{e}}_r^{QM} = \bar{\dot{e}}_r^{2PN} = 0. \tag{8}$$

As expected, the average shape of the orbit does not change when dissipation by gravitational waves is neglected.

C. Euler angles

These evolutions are nontrivial, as discussed below.

1. Inclination α

The secular evolution of the inclination $\alpha = \arccos(\hat{\mathbf{J}}\cdot\hat{\mathbf{L}}_\mathbf{N})$ emerges as the sum of the contributions:

$$\bar{\dot{\alpha}}^{PN} = 0, \tag{9}$$

$$\bar{\dot{\alpha}}^{SO} = \frac{\eta\pi}{\mathfrak{T}\bar{\mathfrak{l}}_r^3}\sum_{k=1}^{2}(4\nu^{2k-3}+3)\chi_k \sin\kappa_k \cos(\psi_p + \zeta_k), \tag{10}$$

$$\bar{\dot{\alpha}}^{SS} = -\frac{3\eta\pi}{\mathfrak{T}\bar{\mathfrak{l}}_r^4}\chi_1\chi_2[\sin\kappa_1\cos\kappa_2\cos(\psi_p+\zeta_1) + \cos\kappa_1\sin\kappa_2\cos(\psi_p+\zeta_2)], \tag{11}$$

$$\bar{\dot{\alpha}}^{QM} = -\frac{3\eta\pi}{2\mathfrak{T}\bar{\mathfrak{l}}_r^4}\sum_{k=1}^{2}\nu^{2k-3}w_k\chi_k^2\sin 2\kappa_k\cos(\psi_p+\zeta_k). \tag{12}$$

$$\bar{\dot{\alpha}}^{2PN} = 0. \tag{13}$$

As expected, the inclination only changes due to spin and quadrupolar effects.

2. Longitude of the ascending node $-\phi_n$

The longitude of the ascending node $-\phi_n$ is subtended by the inertial axis $\hat{\mathbf{x}}$ and the ascending node $\hat{\mathbf{l}} = \hat{\mathbf{L}}_\mathbf{N} \times \hat{\mathbf{J}}$. It has the following contributions to its secular evolution:

$$\bar{\dot{\phi}}_n^{PN} = 0, \tag{14}$$

$$\bar{\dot{\phi}}_n^{SO} = -\frac{\eta\pi}{\mathfrak{T}\bar{\mathfrak{l}}_r^3\sin\alpha}\sum_{k=1}^{2}(4\nu^{2k-3}+3)\chi_k\sin\kappa_k\sin(\psi_p+\zeta_k), \tag{15}$$

$$\bar{\dot{\phi}}_n^{SS} = \frac{3\eta\pi}{\mathfrak{T}\bar{\mathfrak{l}}_r^4\sin\alpha}\chi_1\chi_2[\sin\kappa_1\cos\kappa_2\sin(\psi_p+\zeta_1) + \cos\kappa_1\sin\kappa_2\sin(\psi_p+\zeta_2)], \tag{16}$$

$$\bar{\dot{\phi}}_n^{QM} = \frac{3\eta\pi}{2\mathfrak{T}\bar{\mathfrak{l}}_r^4\sin\alpha}\sum_{k=1}^{2}\nu^{2k-3}w_k\chi_k^2\sin 2\kappa_k\sin(\psi_p+\zeta_k), \tag{17}$$

$$\bar{\dot{\phi}}_n^{2PN} = 0. \tag{18}$$

Again, only spin and quadrupolar effects contribute.

3. Argument of the periastron ψ_p

The secular evolution of ψ_p, the angle between the node line ($\hat{\mathbf{l}}$, perpendicular to both $\mathbf{L_N}$ and $\mathbf{J}$) and the periastron ($\hat{\mathbf{A}}_\mathbf{N}$), is the sum of

$$\bar{\dot{\psi}}_p^{PN} = \frac{6\pi}{\mathfrak{T}\bar{\mathfrak{l}}_r^2}, \tag{19}$$

$$\bar{\dot{\psi}}_p^{SO} = -\frac{\eta\pi}{\mathfrak{T}\bar{\mathfrak{l}}_r^3}\sum_{k=1}^{2}(4\nu^{2k-3}+3) \times \chi_k[2\cos\kappa_k + \cot\alpha\,\sin\kappa_k\sin(\psi_p+\zeta_k)], \tag{20}$$

$$\bar{\psi}_p^{SS} = \frac{3\eta\pi}{\mathfrak{T}\bar{\mathfrak{l}}_r^4}\chi_1\chi_2\{\cot\alpha[\sin\kappa_1\cos\kappa_2\sin(\psi_p+\zeta_1) + \cos\kappa_1\sin\kappa_2\sin(\psi_p+\zeta_2)] + 2\cos\kappa_1\cos\kappa_2 - \sin\kappa_1\sin\kappa_2\cos(\zeta_2-\zeta_1)\}, \quad (21)$$

$$\bar{\psi}_p^{QM} = \frac{3\eta\pi}{2\mathfrak{T}\bar{\mathfrak{l}}_r^4}\sum_{k=1}^{2}\nu^{2k-3}w_k\chi_k^2[\cot\alpha\sin 2\kappa_k\sin(\psi_p+\zeta_k) - 3\sin^2\kappa_k + 2], \quad (22)$$

$$\bar{\psi}_p^{2PN} = \frac{3\pi}{2\mathfrak{T}\bar{\mathfrak{l}}_r^4}[33\bar{e}_r^2 - 4\eta - 6\bar{e}_r^2\eta + 2]. \quad (23)$$

All PN, spin, and quadrupolar corrections lead to periastron precession.

D. Spin angles

The contributions to the secular evolutions of the spin polar angles κ_i and the azimuthal angles ζ_i are

$$\bar{\kappa}_i^{PN} = 0, \quad (24)$$

$$\bar{\kappa}_i^{SO} = \frac{\eta\pi}{\mathfrak{T}\bar{\mathfrak{l}}_r^3}(4\nu^{2j-3}+3)\chi_j\sin\kappa_j\sin(\zeta_i-\zeta_j), \quad (25)$$

$$\bar{\kappa}_i^{SS} = -\frac{\eta\pi}{\mathfrak{T}\bar{\mathfrak{l}}_r^4}\chi_j\sin\kappa_j\sin(\zeta_i-\zeta_j)(\bar{\mathfrak{l}}_r\nu^{2j-3}+3\chi_i\cos\kappa_i), \quad (26)$$

$$\bar{\kappa}_i^{QM} = -\frac{3\eta\pi}{2\mathfrak{T}\bar{\mathfrak{l}}_r^4}\nu^{2j-3}w_j\chi_j^2\sin 2\kappa_j\sin(\zeta_i-\zeta_j), \quad (27)$$

$$\bar{\kappa}_i^{2PN} = 0, \quad (28)$$

$$\bar{\zeta}_i^{PN} = -\bar{\psi}_p^{PN}, \quad (29)$$

$$\bar{\zeta}_i^{SO} = \frac{\eta\pi}{\mathfrak{T}\bar{\mathfrak{l}}_r^3}\{\bar{\mathfrak{l}}_r(4+3\nu^{3-2i}) + 3(4\nu^{2i-3}+3)\chi_i\cos\kappa_i + (4\nu^{2j-3}+3)\chi_j \times[2\cos\kappa_j + \cot\kappa_i\sin\kappa_j\cos(\zeta_i-\zeta_j)]\}, \quad (30)$$

$$\bar{\zeta}_i^{SS} = -\frac{\eta\pi}{\mathfrak{T}\bar{\mathfrak{l}}_r^3}\nu^{2j-3}\chi_j[2\cos\kappa_j+\cot\kappa_i\sin\kappa_j\cos(\zeta_i-\zeta_j)] - \frac{3\eta\pi}{\mathfrak{T}\bar{\mathfrak{l}}_r^4}\chi_i\chi_j\{\cot\kappa_i[3\sin\kappa_i\cos\kappa_j+\cos\kappa_i\sin\kappa_j\cos(\zeta_i-\zeta_j)] - \sin\kappa_i\sin\kappa_j\cos(\zeta_i-\zeta_j)\}, \quad (31)$$

$$\bar{\zeta}_i^{QM} = -\frac{3\eta\pi}{\mathfrak{T}\bar{\mathfrak{l}}_r^3}w_i\chi_i\cos\kappa_i - \frac{3\eta\pi}{2\mathfrak{T}\bar{\mathfrak{l}}_r^4}\sum_{k=1}^{2}w_k\nu^{2k-3}\chi_k^2 \times[2-3\sin^2\kappa_k+\cot\kappa_i\sin(2\kappa_k)\cos(\zeta_i-\zeta_k)], \quad (32)$$

$$\bar{\zeta}_i^{2PN} = -\bar{\psi}_p^{2PN}. \quad (33)$$

Here, $i \neq j$, and $i = 1, 2$.

It is easy to check that in the binary black hole case the dynamics indeed provides the additional constant of motion found by Racine [21], which in our notation becomes

$$\xi = \frac{G\mu m}{c}[(1+\nu^{-1})\chi_1\cos\kappa_1 + (1+\nu)\chi_2\cos\kappa_2]. \quad (34)$$

Its time derivative indeed vanishes as can be seen by employing Eqs. (24)–(28) with $w_i = 1$. However, there is no obvious way to generalize this constant for arbitrary quadrupole parameter $w_i \neq 1$.

E. Secular precession angular velocities

The averaged precession angular velocities are calculated from Eqs. (31)–(33) of Ref. [59][2]:

$$\overline{\omega_{\mathbf{i}}\cdot\hat{\mathbf{A}}_{\mathbf{N}}} = \frac{2\eta\pi}{\mathfrak{T}\bar{\mathfrak{l}}_r^3}(\nu^{2j-3}\chi_j\sin\kappa_j\cos\zeta_j + 3w_i\chi_i\sin\kappa_i\cos\zeta_i) \quad (35)$$

$$\overline{\omega_{\mathbf{i}}\cdot\hat{\mathbf{Q}}_{\mathbf{N}}} = \frac{2\eta\pi}{\mathfrak{T}\bar{\mathfrak{l}}_r^3}(\nu^{2j-3}\chi_j\sin\kappa_j\sin\zeta_j + 3w_i\chi_i\sin\kappa_i\sin\zeta_i) \quad (36)$$

$$\overline{\omega_{\mathbf{i}}\cdot\hat{\mathbf{L}}_{\mathbf{N}}} = \frac{\eta\pi}{\mathfrak{T}\bar{\mathfrak{l}}_r^3}[\bar{\mathfrak{l}}_r(4+3\nu^{3-2i}) + 2\nu^{2j-3}\chi_j\cos\kappa_j]. \quad (37)$$

It is easy to see by checking the leading-order term of $\mathfrak{T}$ that as $\bar{e}_r$ goes to 1 the precession becomes increasingly small. It is explained by the fact that on parabolic orbits, when $\bar{e}_r = 1$, the motion becomes unbound, and there is no well-defined period, thus no precession.

F. Constraints

The 2PN dynamics of compact binaries (given by Eqs. (36)–(45) of Ref. [59]) have four first integrals which are derived in Secs. V.A. and V.B. of Ref. [59]. The first integrals give the conservation of total energy and total angular momentum. Two first integrals which express the direction of total angular momentum and given by Eq. (53) and the ratio of Eqs. (54) and (55) of Ref. [59] represent two constraints among the variables occurring in the secular evolution equations. As a result of this, the secular dynamics given above is subject to two constraints among the shape variables, the Euler angles, and spin angles, which will be shown below.

[2]In Eqs. (B34) of Ref. [58], the SS and QM terms have typos: the 1/2 factors should be removed. We thank Krisztina Kövér for pointing this out. Because of this, the second term of Eq. (33) of Ref. [59] contains unnecessary 1/2 factors on the rhs (but otherwise all conclusions remain unchanged). In the present paper, these have been corrected, and both the instantaneous and secular dynamics are represented correctly.

The constraints determining the direction of the total angular momentum to leading order (see Eqs. (58) and (62) of Ref. [59]) read as

$$\bar{\mathfrak{l}}_r = \sum_{i=1}^{2} \nu^{2i-3}\chi_i[\sin\kappa_i \sin(\zeta_i + \psi_p)\cot\alpha - \cos\kappa_i], \tag{38}$$

and

$$\sum_{i=1}^{2} \nu^{2i-3}\chi_i \sin\kappa_i \cos(\zeta_i + \psi_p) = 0. \tag{39}$$

Here, $\mathfrak{l}_r(\chi_p)$ was changed to $\bar{\mathfrak{l}}_r$, an approximation valid to leading order. These expressions do not depend explicitly on the variable χ_p characterizing the position of the body with reduced mass. Only the correction terms $\mathcal{O}(\bar{\mathfrak{l}}_r^{-2})$ to the above equations exhibit explicit χ_p dependence. Therefore, we expect the constraints (38) and (39) to be conserved under the secular evolution.

Since $\bar{\mathfrak{l}}_r$ is a constant, the time derivative of the left-hand side of (38) is zero. A long but straightforward computation with the application of the secular evolution equations shows that the time derivative of the right-hand side also vanishes. Similarly, we checked that the time derivative of Eq. (39) vanishes to 2PN order. These prove that Eqs. (38) and (39) are first integrals of the secular evolution equations given in Secs. II B–II D. They can be used to reduce the order of the differential equation system or for checking the accuracy of the numerical integration. In addition, Eqs. (38) and (39) have to be fulfilled when setting up initial conditions.

III. SECULAR AND INSTANTANEOUS DYNAMICS OF BLACK HOLE BINARIES COMPARED

A. Conservative timescale

Because of gravitational radiation, the PN parameter increases during the inspiral. During the time

$$\Delta\tau = \frac{5}{256\eta}(\varepsilon_{(\mathrm{in})}^{-4} - \varepsilon_{(\mathrm{out})}^{-4})\frac{Gm}{c^3}, \tag{40}$$

the PN parameter evolves from $\varepsilon_{(\mathrm{in})}$ to $\varepsilon_{(\mathrm{out})}$ [25]. For numerical evolution purposes, we define the dimensionless conservative timescale $\tilde{\mathfrak{T}}_{\mathrm{cons}}$ as a 1% increase in the PN parameter:

$$\tilde{\mathfrak{T}}_{\mathrm{cons}} = \frac{5}{256\eta}\varepsilon_{(\mathrm{in})}^{-4}\left(1 - \frac{1}{1.01^4}\right) \approx \frac{0.195}{256\eta}\varepsilon_{(\mathrm{in})}^{-4}. \tag{41}$$

Dividing this by (the leading-order dimensionless) orbital period $\tilde{\mathfrak{T}}_{\mathrm{orb}} = 2\pi\varepsilon^{-3/2}$ gives the number

$$N_{\mathrm{max}} = \frac{0.195}{512\pi\eta}\varepsilon_{(\mathrm{in})}^{-5/2} \tag{42}$$

of radial periods of the conservative timescale. Evolving numerically for N_{max} periods keeps the error of disregarding the dissipation below 1%.

B. Accuracy of the secular dynamics

We check the long-term accuracy of the secular dynamics by a numerical comparison over N_{max} periods with the instantaneous evolutions given by Eqs. (36)–(42) of Ref. [59]. The results are shown on Figs. 1–4. All figures are for $m = 20\,M_\odot$, $\nu = 1/2$, and high-spin parameter values $\chi_1 = \chi_2 = 0.9982$. The initial value for the PN parameter is $\varepsilon(0) = 10^{-2}$ in Figs. 1 and 2, while $\varepsilon(0) = 5\times10^{-4}$ in Figs. 3 and 4. The initial value for the eccentricity is $e_r(0) = 0.1$ in Figs. 1 and 3 and $e_r(0) = 0.5$ in Figs. 2 and 4.

For the instantaneous evolutions, the shape parameter $\mathfrak{l}_r(0)$ emerged from the PN parameter $\varepsilon(0)$ and eccentricity $e_r(0)$ cf. Eq. (8) of Ref. [59]. Then, $\psi_p(0)$ and $\alpha(0)$ were computed from the constraints given by Eq. (53) and the ratio of Eqs. (54) and (55) of Ref. [59].

The initial values $\bar{f}(0)$ for the secular dynamics were extracted from the instantaneous evolution during the first orbit in the following manner,

$$\bar{f}(0) = \bar{f} - \frac{1}{2}[f(\mathfrak{T}) - f(0)], \tag{43}$$

where $\bar{f}$ represents the first orbital average. This method corrects for the periodic component of the instantaneous motion, leading to the proper initial condition for the secular evolution representing the orbital average.

In the secular dynamics, the shape variables $\bar{e}_r$ and $\bar{\mathfrak{l}}_r$ are conserved. Finally, the initial values of ψ_p and α were computed from the constraints (38) and (39).

The smaller pictures zoom into the first two radial periods of the evolution. On the conservative timescale, the secular evolution follows closely the instantaneous evolutions. Certain evolutions even overlap, making them hard to distinguish.

C. Effects of the eccentricity and PN parameter

The comparison of Figs. (1) and (2), and also (3) and (4), yields to the remark that N_{max} decreases with increasing eccentricity, whereas comparing the evolutions of distant binaries in Figs. (2) and (4) to the close binary evolutions (1) and (3) yields that N_{max} decreases with increasing PN parameter.

While Figs. (3) and (4) represent the early stages of the inspiral, Figs. (1) and (2) refer to the very end of it. While the secular evolution of the spin azimuthal angles $\zeta_{1,2}$ indicate more than 60 precessional cycles at low eccentricity and more than 20 for high eccentricity in the early inspiral regime, at the end of it, N_{max} will not reach even one single precessional cycle. Similarly, the number of nutations (represented by the number of cycles of the polar

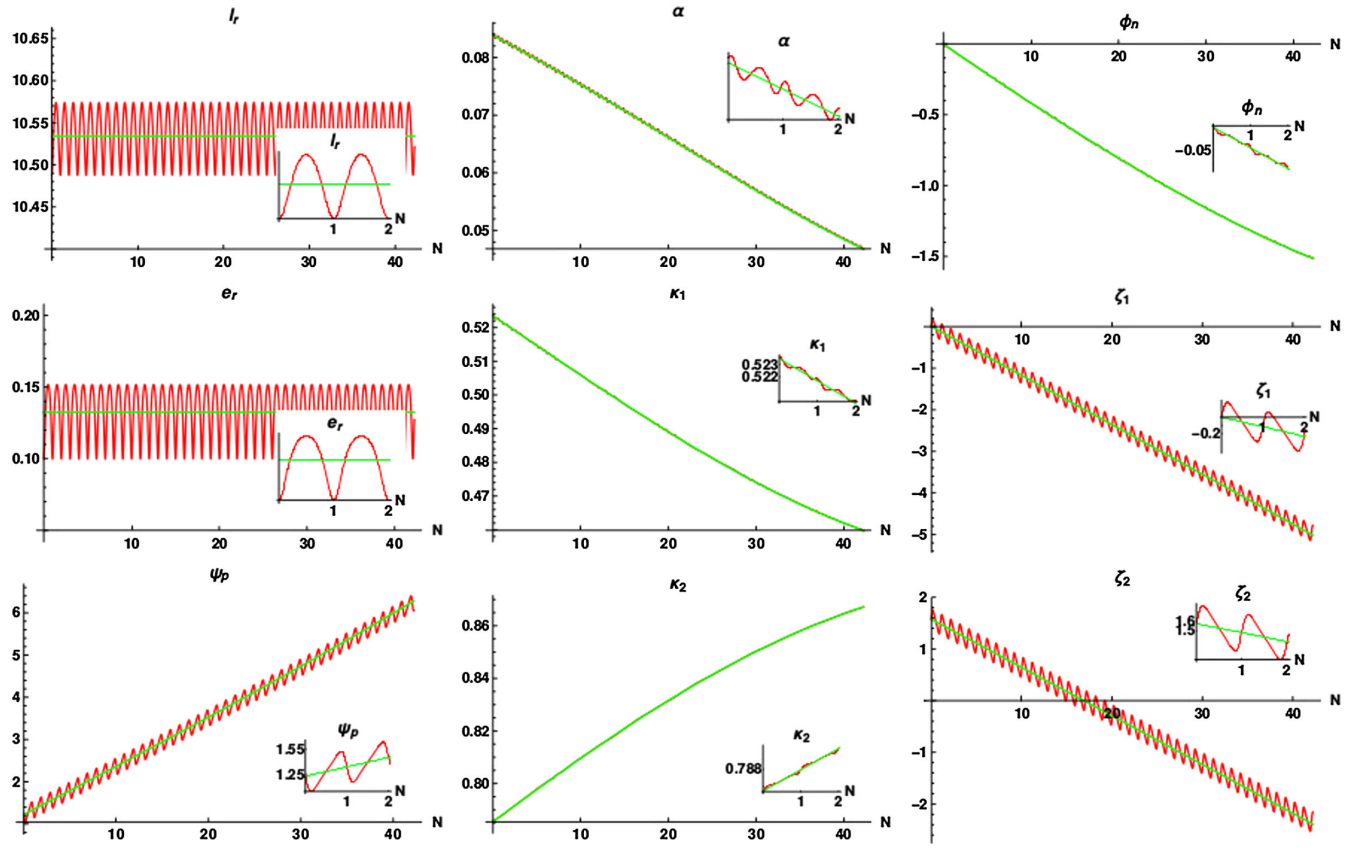

FIG. 1. The panels represent the secular (green) and instantaneous (red) evolutions of $\mathfrak{l}_r$, e_r, α, ϕ_n, ψ_p, κ_i, and ζ_i $(i=1,2)$ as functions of the number of orbital periods N. The parameters and initial conditions for the instantaneous evolutions are total mass $m=20\,M_\odot$, mass ratio $\nu=0.5$, dimensionless spin parameters $\chi_1=\chi_2=0.9982$, eccentricity $e_r(0)=0.1$, spin polar angles $\kappa_1(0)=\pi/6$ and $\kappa_2(0)=\pi/4$, spin azimuthal angles $\zeta_1(0)=0$ and $\zeta_2(0)=\pi/2$, longitude of the ascending node $\phi_n(0)=0$, and post-Newtonian parameter $\varepsilon(0)=0.01$. Matching initial conditions for the secular dynamics have been chosen, as explained in the main text. On some of the plots, the two evolutions overlap at the chosen resolution. On each panel, the first two periods are also shown in order to illustrate that the match only occurs on the longer run.

angles κ_i between their maximal and minimal values) is 18 at low eccentricity and 5 at high eccentricity in the early inspiral, while at the end of it, $N_{\max}$ covers only a fraction of the nutational period. The polar angle α and azimuthal angle ϕ_n of the orbital angular momentum exhibit similar behavior to that of the spins.

IV. CLOSED SYSTEM FOR THE SECULAR SPIN ANGLE EVOLUTIONS

Remarkably, the secular evolution of the spin angles κ_1 and κ_2 and $\Delta\zeta\equiv\zeta_1-\zeta_2$ discussed in Sec. II form a closed subset:

$$\frac{1}{R}\overline{\frac{d\kappa_1}{d\mathfrak{t}}}=(1+\nu-x_1\cos\kappa_1-\nu w_2x_2\cos\kappa_2)x_2\sin\kappa_2\sin\Delta\zeta, \tag{44}$$

$$\frac{1}{R}\overline{\frac{d\kappa_2}{d\mathfrak{t}}}=-(1+\nu^{-1}-x_2\cos\kappa_2-\nu^{-1}w_1x_1\cos\kappa_1)\times x_1\sin\kappa_1\sin\Delta\zeta, \tag{45}$$

$$\begin{aligned}\frac{1}{R}\overline{\frac{d\Delta\zeta}{d\mathfrak{t}}}=&\nu-\nu^{-1}+(1+2\nu^{-1}-w_1-w_1\nu^{-1}x_1\cos\kappa_1)x_1\cos\kappa_1\\&-(1+2\nu-w_2-w_2\nu x_2\cos\kappa_2)x_2\cos\kappa_2\\&-(1+\nu^{-1}-w_1\nu^{-1}x_1\cos\kappa_1)x_1\cot\kappa_2\sin\kappa_1\cos\Delta\zeta\\&+(1+\nu-w_2\nu x_2\cos\kappa_2)x_2\cot\kappa_1\sin\kappa_2\cos\Delta\zeta\\&-x_1x_2\left(\frac{\sin\kappa_2}{\sin\kappa_1}-\frac{\sin\kappa_1}{\sin\kappa_2}\right)\cos\Delta\zeta,\end{aligned} \tag{46}$$

where we have introduced the notations

$$R=\frac{3\eta\pi}{\mathfrak{T}\bar{\mathfrak{l}}_r^2},\qquad x_i=\frac{\chi_i}{\bar{\mathfrak{l}}_r}. \tag{47}$$

In Appendix B, we prove that the evolutions remain regular across manifest coordinate singularities.

In the next two sections, we will discuss applications for this closed system.

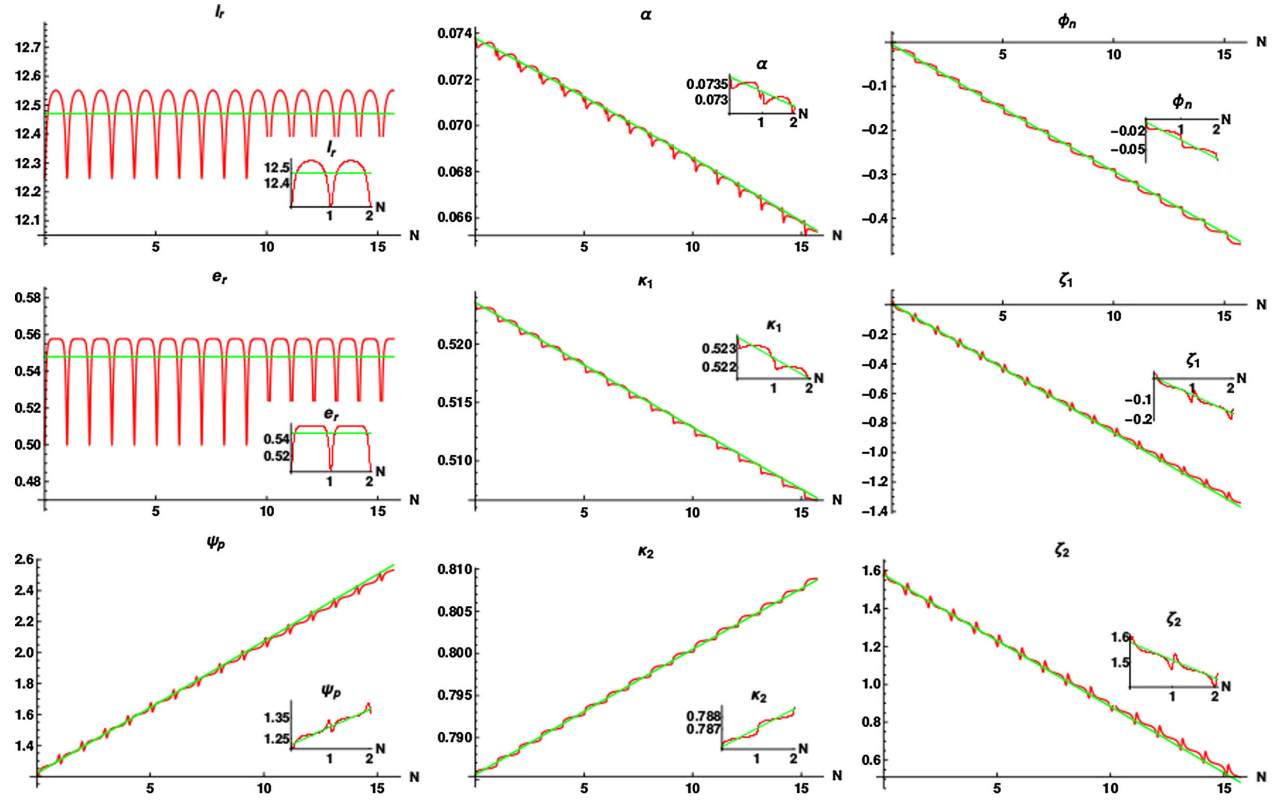

FIG. 2. The effect of an increased eccentricity $e_r(0) = 0.5$, the rest of the parameters being identical to those for Fig. 1.

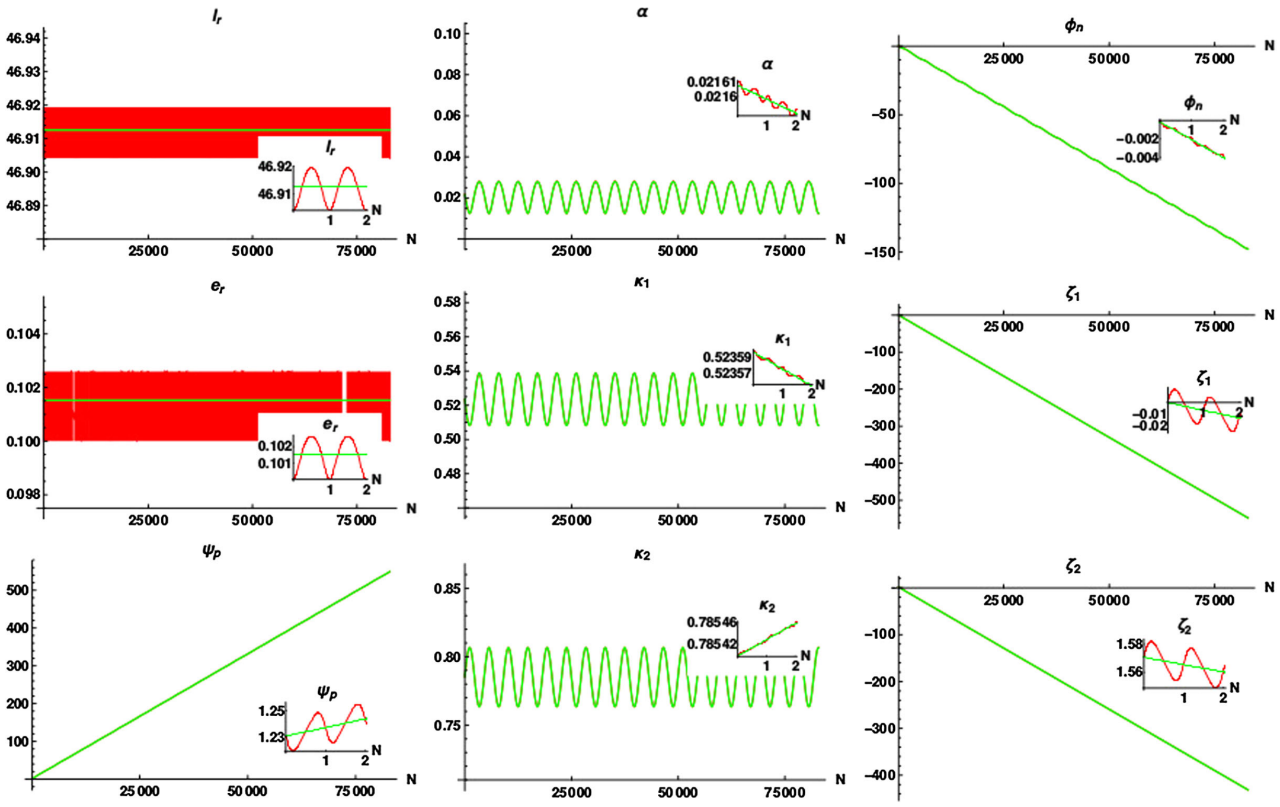

FIG. 3. The evolutions at a much earlier stage of the inspiral, characterized by post-Newtonian parameter $\varepsilon(0) = 0.0005$, the rest of the parameters being identical to those for Fig. 1.

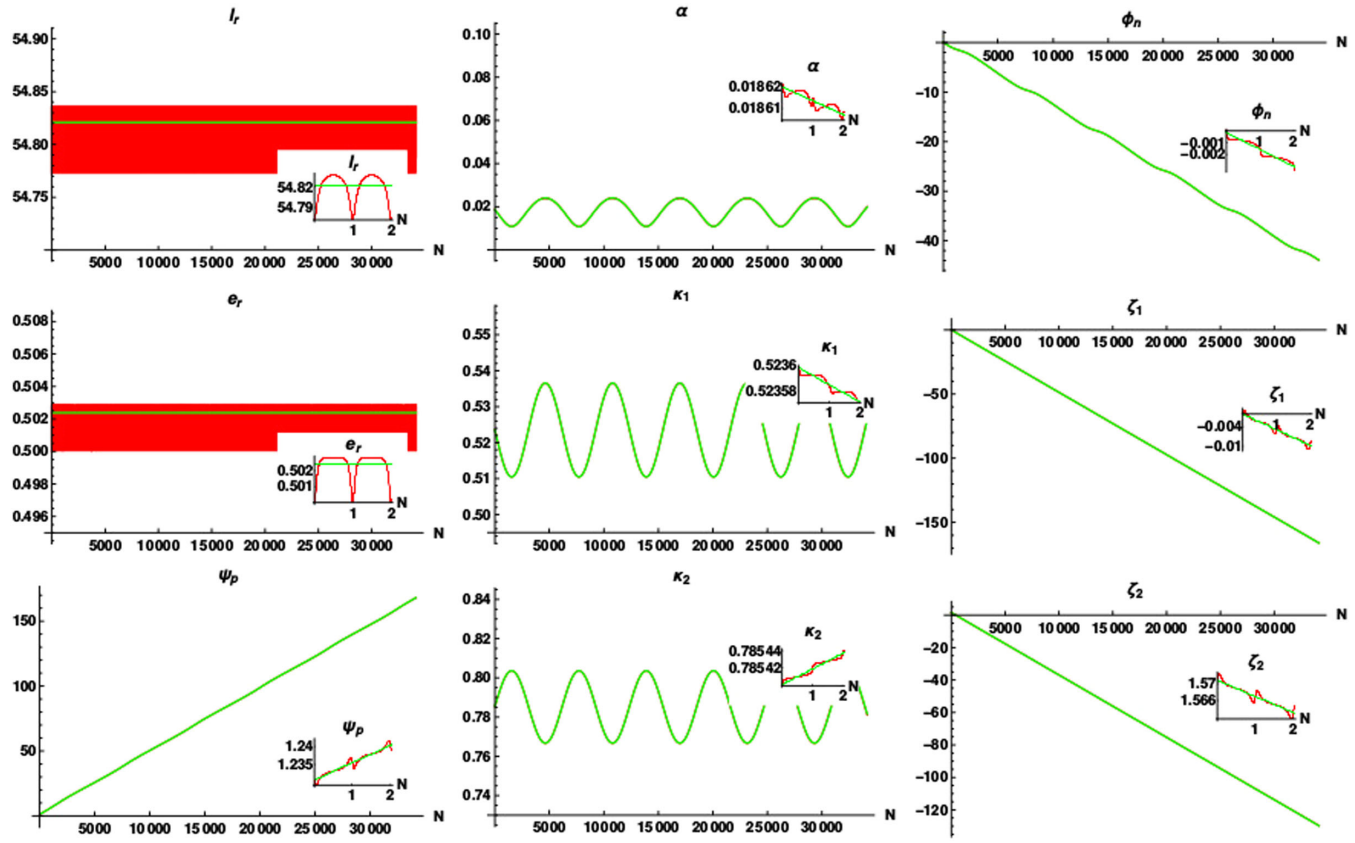

FIG. 4. The effect of an increased eccentricity $e_r(0) = 0.5$, the rest of the parameters being identical to those for Fig. 3.

V. SPIN FLIP-FLOPS WHEN ONE SPIN DOMINATES OVER THE OTHER

In this section, we consider the case of one spin dominating over the other, thus $\chi_2 \ll \chi_1$. Under these conditions, we will recover configurations with large spin flip-flop already discussed in the literature and an additional flip-flop induced by a particular value of the quadrupole parameter, relevant for neutron star binaries.

Since

$$\mathcal{O}\left(\overline{\frac{d\kappa_1}{d\mathfrak{t}}}\right)\Big/\mathcal{O}\left(\overline{\frac{d\kappa_2}{d\mathfrak{t}}}\right) \approx \frac{\nu\chi_2}{\chi_1} \ll 1, \tag{48}$$

in this case, κ_1 behaves as a quasiconstant. The system governing $\Delta\zeta$ and κ_2 simplifies to

$$\overline{\frac{d\Delta\zeta}{d\mathfrak{t}}} = A_{S_1} + B_{S_1}\cot\kappa_2\cos\Delta\zeta, \tag{49}$$

$$\overline{\frac{d\kappa_2}{d\mathfrak{t}}} = B_{S_1}\sin\Delta\zeta, \tag{50}$$

with coefficients

$$\frac{A_{S_1}}{R} = \nu - \frac{1}{\nu} + \left(1 + \frac{2}{\nu} - w_1 - \frac{w_1 x_1}{\nu}\cos\kappa_1\right) x_1\cos\kappa_1, \tag{51}$$

and

$$\frac{B_{S_1}}{R} = -\left(1 + \frac{1}{\nu} - \frac{w_1 x_1}{\nu}\cos\kappa_1\right) x_1\sin\kappa_1. \tag{52}$$

For the values $\kappa_1 = \{0, \pi\}$, the angle κ_2 becomes a constant, and $\Delta\zeta = A_{S_1}\mathfrak{t} + \text{constant}$.

For generic κ_1, the system has fix points given by $\overline{d\Delta\zeta}/d\mathfrak{t} = 0$ and $\overline{d\kappa_2}/d\mathfrak{t} = 0$, resulting in either

$$\Delta\zeta = 0, \qquad \kappa_2 = \arctan\left(-\frac{B_{S_1}}{A_{S_1}}\right) \tag{53}$$

or

$$\Delta\zeta = \pi, \qquad \kappa_2 = \arctan\left(\frac{B_{S_1}}{A_{S_1}}\right). \tag{54}$$

In the rest of the cases [other than $\kappa_1 = \{0, \pi\}$ or the fix points (53) or (54)], we derive the following second-order differential equation from Eqs. (49)–(50),

$$\overline{\frac{d^2}{d\mathfrak{t}^2}}(\sin\kappa_2\sin\Delta\zeta) + \Omega_{S_1}^2\sin\kappa_2\sin\Delta\zeta = 0, \tag{55}$$

where

$$\Omega_{S_1} = \sqrt{A_{S_1}^2 + B_{S_1}^2}. \tag{56}$$

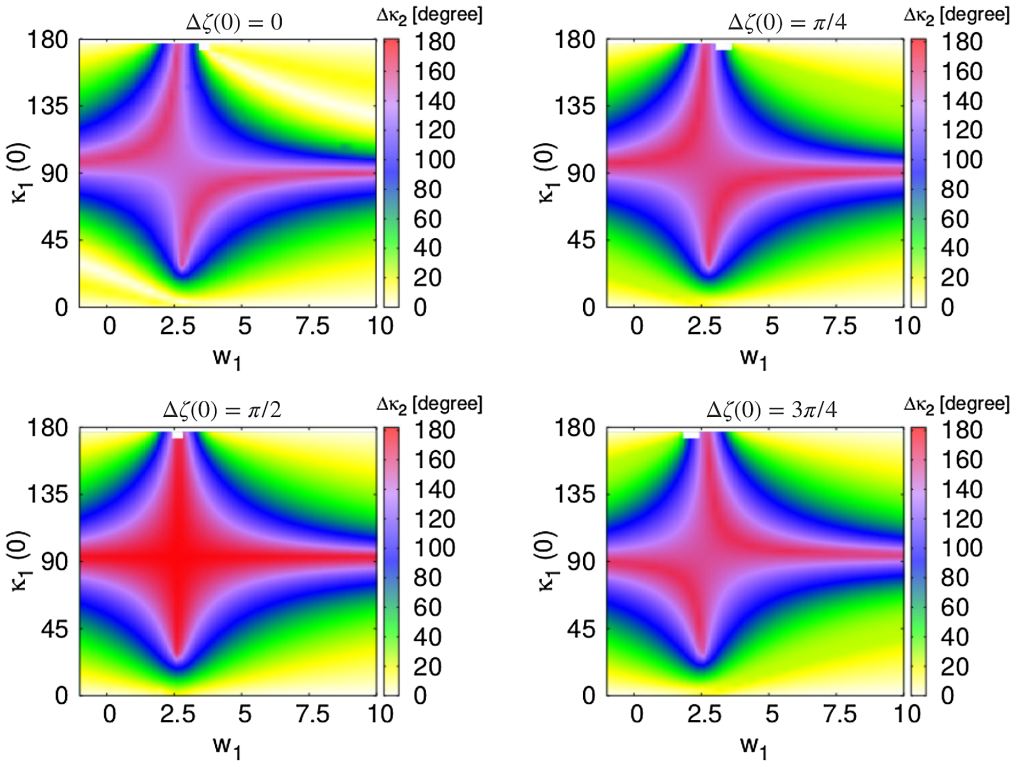

FIG. 5. The color map represents the flip-flop angle $\Delta\kappa_2$ as a function of the initial polar angle $\kappa_1(0)$ and the quadrupole parameter w_1 of the dominant spin ($\chi_1 \gg \chi_2$). From the top left to lower right panel, $\Delta\zeta(0)$ is 0, $\pi/4$, $\pi/2$, and $3\pi/4$, respectively. The additional parameters of the binary are $m_1 = m_2 = 1.4\ M_\odot$, $\bar{e}_r = 0.1$, $\bar{\epsilon} = 0.0001$, $\chi_1 = 0.95$, $\chi_2 = 0.05$, and $\kappa_2(0) = \pi/10$. In the small white rectangle regions, $\Delta\kappa_2$ does not reach its maximum within the conservative timescale. The flip-flop is large in the red diamond-shaped regions.

Equation (55) represents a harmonic oscillator, and its solution reads

$$\sin\kappa_2 \sin\Delta\zeta = K_1 \cos\left(\Omega_{S_1}\bar{\mathrm{t}} + D_{S_1}\right), \tag{57}$$

with integration constants $|K_1| \leq 1$ and D_{S_1}. Then, from (50), we obtain

$$\cos\kappa_2 = -\frac{K_1 B_{S_1}}{\Omega_{S_1}} \sin\left(\Omega_{S_1}\bar{\mathrm{t}} + D_{S_1}\right) + K_2, \tag{58}$$

where $|K_2| \leq 1$ is an additional integration constant. Since the system (49)–(50) of two first-order differential equations admits only two integration constants, K_1, K_2, and D_{S_1} are not independent. Indeed, by taking the derivative of Eq. (57) and using Eqs. (49)–(50) and (58), we find that

$$A_{S_1} \sin\kappa_2 \cos\Delta\zeta = \frac{A_{S_1}^2}{B_{S_1}} \cos\kappa_2 - \frac{\Omega_{S_1}^2}{B_{S_1}} K_2. \tag{59}$$

Hence, $A_{S_1} = 0$ also implies $K_2 = 0$. We introduce a new constant C as

$$K_2 = A_{S_1} C \tag{60}$$

with arbitrary value for $A_{S_1} = 0$ and from (59) and (57)–(58),

$$K_1^2 = 1 - \Omega_{S_1}^2 C^2, \tag{61}$$

otherwise. Hence, the solutions (57) and (58) can be rewritten as

$$\cos\kappa_2 = A_{S_1} C + \frac{\epsilon B_{S_1}}{\Omega_{S_1}} \sqrt{1 - \Omega_{S_1}^2 C^2} \sin\left(\Omega_{S_1}\bar{\mathrm{t}} + D_{S_1}\right), \tag{62}$$

$$\sin\kappa_2 \sin\Delta\zeta = -\epsilon \sqrt{1 - \Omega_{S_1}^2 C^2} \cos\left(\Omega_{S_1}\bar{\mathrm{t}} + D_{S_1}\right), \tag{63}$$

where $\epsilon = \pm 1$ and $-\epsilon$ gives the sign of K_1.[3]

From Eq. (62), the maximal variation of $\cos\kappa_2$ during the evolution is

$$\begin{aligned} |\Delta\cos\kappa_2| &= \left| \frac{2B_{S_1}}{\Omega_{S_1}} \sqrt{1 - \Omega_{S_1}^2 C^2} \right| \\ &= \left| 2\sqrt{\frac{B_{S_1}^2}{A_{S_1}^2 + B_{S_1}^2} - B_{S_1}^2 C^2} \right|. \end{aligned} \tag{64}$$

[3]Note that the reverse case $\chi_1 \ll \chi_2$ can be obtained by the following notational changes: $\chi_1 \to \chi_2$, $\nu \to \nu^{-1}$, $w_1 \to w_2$, $\kappa_1 \to \kappa_2$, and $\Delta\zeta \to -\Delta\zeta$.

This is the largest when

$$A_{S_1}^2 \ll B_{S_1}^2. \tag{65}$$

As $x_1 = \chi_1/\bar{\mathfrak{l}}_r$ and $1/\bar{\mathfrak{l}}_r$ represents 1/2PN order (Ref. [59]), a necessary condition for Eq. (65) is $\nu \approx 1$, since in this case the leading-order term of $A_{S_1}^2$ is negligible. Further the condition (65), implying a large change in the polar angle of the smaller spin cf. Eq. (64), holds in two cases,

$$i) \quad \cos\kappa_1 = \mathcal{O}\left(\frac{1}{\bar{\mathfrak{l}}_r}\right), \tag{66}$$

and

$$ii) \quad 1 + \frac{2}{\nu} - w_1 - \frac{w_1 x_1}{\nu}\cos\kappa_1 = \mathcal{O}\left(\frac{1}{\bar{\mathfrak{l}}_r}\right). \tag{67}$$

The condition (66) means that the larger spin vector is almost perpendicular to $\mathbf{L}_N$ (with a deviation of 1/4PN order allowed). This configuration, which results in large flip-flops of the smaller spin, was analyzed first in Ref. [35] for quasicircular orbits. By contrast, as κ_1 is contained in a $\mathcal{O}(1/\bar{\mathfrak{l}}_r)$ term of Eq. (67), the second condition could hold for a wide range of angles κ_1 (i.e., almost independently of the direction of the dominant spin), provided the binary component with dominant spin has a quadrupole moment $w_1 \approx 3$. This situation can be relevant for neutron star - neutron star binary systems where one of the binary components is spinning much faster than the other. Both flip-flop situations arising under i) and ii) are represented on Fig. 5 in a combined fashion as the red diamond-shaped regions. Case i) occurs along the horizontal axis, while case ii) occurs along the vertical one.

VI. BINARIES WITH A BLACK HOLE AND A GRAVASTAR, ANOTHER BLACK HOLE, OR BOSON STAR COMPANION

A. Black hole - boson star binaries

In this subsection, we discuss analytically the case of black hole - boson star binaries with $w_1 = 1$ and $w_2 \approx 100$, also equal masses and at large separations, such that $x_1 \approx x_2 \ll 1$ (as they are of the order of 1/2PN order; also, we assume $w_2 x_2 \ll 1$). The closed system (44)–(46) can be approximated as

$$\frac{1}{R}\overline{\frac{d\kappa_1}{d\mathfrak{t}}} = 2x_2 \sin\kappa_2 \sin\Delta\zeta, \tag{68}$$

$$\frac{1}{R}\overline{\frac{d\kappa_2}{d\mathfrak{t}}} = -2x_1 \sin\kappa_1 \sin\Delta\zeta, \tag{69}$$

$$\frac{1}{R}\overline{\frac{d\Delta\zeta}{d\mathfrak{t}}} = 2x_1\cos\kappa_1 + w_2 x_2 \cos\kappa_2 - 2x_1\cot\kappa_2 \sin\kappa_1 \cos\Delta\zeta + 2x_2 \cot\kappa_1 \sin\kappa_2 \cos\Delta\zeta. \tag{70}$$

The first two equations give

$$\overline{\frac{d\cos\kappa_1}{d\cos\kappa_2}} = -\frac{x_2}{x_1}, \tag{71}$$

or

$$\cos\kappa_2 = \frac{x_1}{x_2}(A - \cos\kappa_1), \tag{72}$$

with A a suitable constant to render $\cos\kappa_2$ in the allowed range. If $\cos\kappa_2 \neq 0$, the first term of Eq. (70) can also be dropped.

In the particular case $A = 0$ and $x_2 = x_1$, Eq. (72) yields $\kappa_2 = \pi - \kappa_1$.

This is a highly symmetrical configuration, with the evolutions of the two spin polar angles occurring symmetrically to the orbital plane. In this setup, Eqs. (68)–(70) reduce to

$$\frac{1}{R}\overline{\frac{d\kappa_1}{d\mathfrak{t}}} = 2x_1 \sin\kappa_1 \sin\Delta\zeta, \tag{73}$$

$$\frac{1}{R}\overline{\frac{d\Delta\zeta}{d\mathfrak{t}}} = -w_2 x_1 \cos\kappa_1. \tag{74}$$

These suitably combined integrate into

$$\cos\Delta\zeta = \ln|C \sin^{\frac{w_2}{2}}\kappa_1|, \tag{75}$$

with C an integration constant. Inserting this into Eq. (73), we obtain an ordinary differential equation,

$$\frac{1}{R}\overline{\frac{d\kappa_1}{d\mathfrak{t}}} = \pm 2x_1 \sin\kappa_1 [1 - (\ln|C\sin^{\frac{w_2}{2}}\kappa_1|)^2]^{1/2}, \tag{76}$$

with formal solution

$$2x_1 R(\mathfrak{t} - \mathfrak{t}_0) = \pm \int \frac{d\kappa_1}{[1 - (\ln|C\sin^{\frac{w_2}{2}}\kappa_1|)^2]^{1/2}\sin\kappa_1}, \tag{77}$$

where $\mathfrak{t}_0$ is another constant. Hence, the time evolution of the spin polar angles is given by Eq. (77), while the evolution of the difference of their azimuthal angles is given by Eq. (75).

B. Comparing flip-flops in black hole - black hole, black hole - gravastar, and black hole - boson star binaries of equal mass

We wish to study here the effect of the quadrupole parameter of the companion compact object to a black hole in the spin flip-flop. The masses of all compact objects were chosen equal; hence, $\nu = 1$. We monitored the evolution at PN parameter $\bar{\varepsilon} = 0.0001$ and eccentricity $\bar{e}_r = 0.1$, leading to $\bar{\mathfrak{l}}_r = 99.5$. We chose the spin

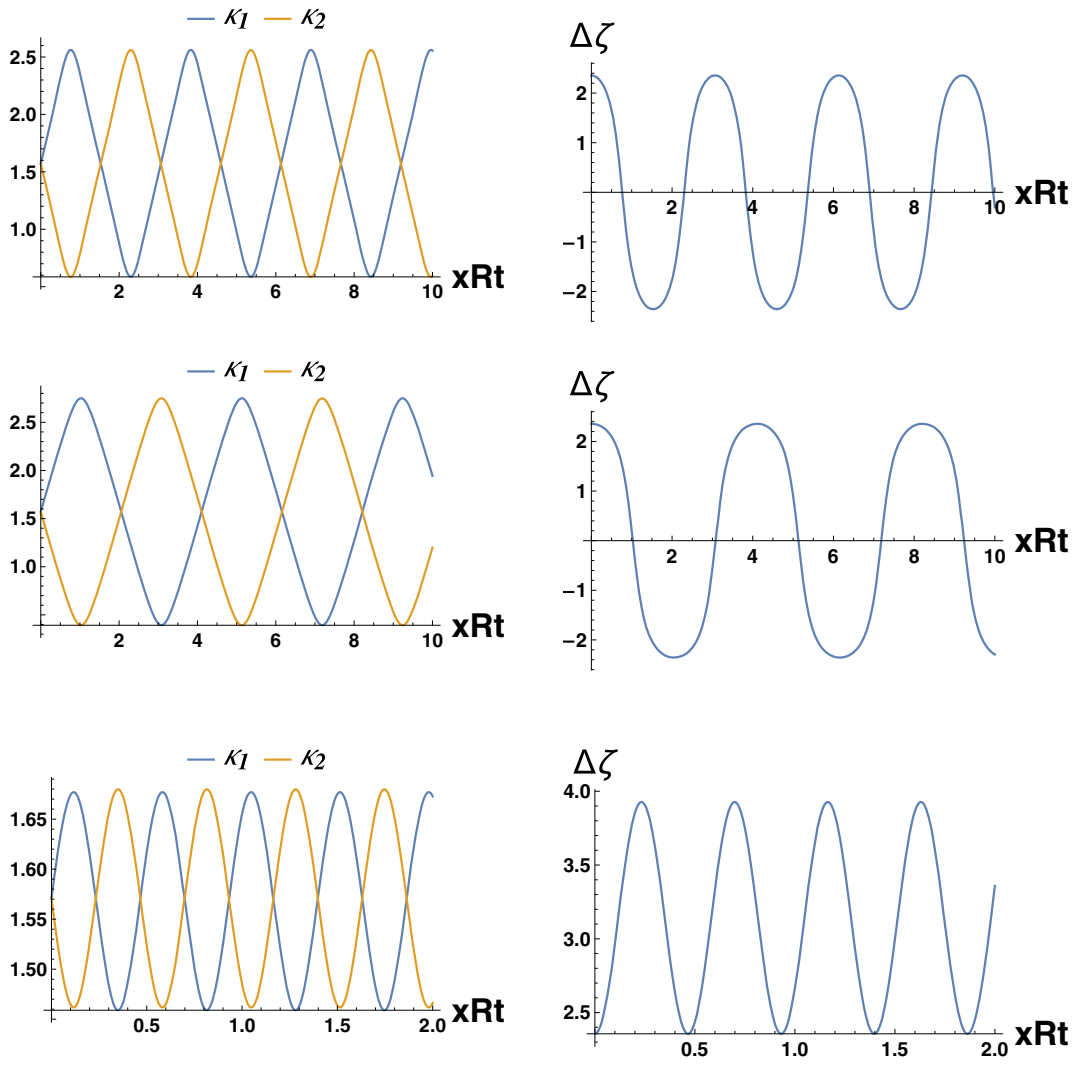

FIG. 6. The evolution of the spin polar angles (left column) and of the difference of their azimuthal angle (right column) as function of the dimensionless time $\mathfrak{t}$ in units of xR, for binaries consisting of a black hole and either a gravastar with $w = -0.8$ (first row), another black hole (second row), or a boson star with $w = 100$ (third row). The mass ratio is $\nu = 1$ in all cases. The plots are for the PN parameter $\bar{\varepsilon} = 0.0001$, eccentricity $\bar{e}_r = 0.1$, the parameters $x \equiv x_1 = x_2 = 0.01$, and initial spin orientations $\kappa_1(0) = \kappa_2(0) = \pi/2$, $\Delta\zeta(0) = 3\pi/4$. The polar angles exhibit a flip-flopping behavior, with both the frequency and amplitude depending on the quadrupole parameter of the compact companion. The difference of the azimuthal angles is also sensitive to w.

magnitudes $\chi_1 = \chi_2 = 0.95$, generating the parameters $x \equiv x_1 = x_2 = 0.01$. For initial values of the spin angles, we picked $\kappa_1(0) = \kappa_2(0) = \pi/2$ (hence, the spins lying in the orbital plane), separated by an azimuthal angle difference of $\Delta\zeta(0) = 3\pi/4$. With these values, we monitored the spin angle evolutions for the three distinct binary systems. The results are represented in Fig. 6.

In all cases, the spin polar angles exhibit the flip-flopping behavior, its amplitude and frequency being affected by the nature of the companion (through the value of the quadrupolar parameter w). We found that the largest amplitude and period occur when the companion is an identical black hole. Both for gravastar and boson star companions, the amplitude and period of the flip-flop decrease. The flip-flop frequency is largely increased for boson star companions. As concerning the difference of the azimuthal angles $\Delta\zeta$, the evolutions are similar for low values of w, thus for gravastar and black hole companions. The spins of the binary components exhibit precessions during which they overpass each other periodically ($\Delta\zeta$ evolves through a sequence of positive and negative values). Nevertheless, when the companion is a boson star, this swinging behavior disappears ($\Delta\zeta$ remains positive). The amplitude of the periodical evolution in $\Delta\zeta$ is also decreased.

VII. CONCLUSIONS

In this paper, we derived the conservative secular evolution of precessing compact binaries on eccentric orbits, to second post-Newtonian–order accuracy, with

leading-order spin-orbit, spin-spin, and mass quadrupole-monopole contributions included. Our approach relies on employing a properly chosen set of dimensionless variables, advanced in Ref. [59] and a method of averaging over the radial period. The secular dynamics emerged by applying this to the instantaneous dynamics discussed in Ref. [59]. The inclusion of the mass quadrupole parameter allows us to apply the formalism for binaries with arbitrary compact components, like black holes, neutron stars, boson stars, or gravastars.

The derived secular dynamics generalizes previous results from the literature. In Ref. [15], the dynamics was only expressed to 1.5PN order by employing different shape variables. In Ref. [30], the precession was examined with leading-order SO and SS effects for orbits with negligible eccentricity. Reference [60] investigates the PN dynamics with eccentricity, but without spins. Reference [68] discusses the dynamics of small mass ratio binaries with only the smaller body having spin. The seminal review on gravitational radiation from compact binary sources by Blanchet [61] discusses the SO effect in its last section but omits the SS and QM contributions to the dynamics. The secular dynamics where the leading-order SO, SS, and QM coupling are included is investigated analytically in Ref. [21] only for black holes.

The secular evolution equations emerged as a closed system of first-order differential equations, which in contrast with the instantaneous evolutions presented in Ref. [59], is autonomous. The dependent variables are the polar (κ_1 and κ_2) and the azimuthal angles (ζ_1 and ζ_2) of the spin vectors, the angles α and ϕ_n giving the orientation of the orbital angular momentum vector, together with the periastron angle ψ_p, the dimensionless magnitude of the orbital angular momentum $\mathfrak{l}_r$, and the eccentricity e_r. Over the conservative timescale, the secular dynamics can be regarded as some sort of smoothed-out intantaneous evolution, as illustrated in Figs. 1–4.

Moreover, we have shown that the spin polar angles and the difference of their azimuthal angles in the system defined by the orbital plane evolve according to a closed subsystem of the secular dynamics. In spite of the apparent singularity of spherical polar coordinates, the evolutions remains well defined through aligned configurations. We studied in detail this closed subsystem in two significant cases. First, we assumed that the masses are comparable, but one of the spins dominates over the other. In this case, we i) derived analytically that large flip-flops of the smaller spin emerge when the larger spin is almost coplanar with the orbit (a known result) and ii) found new flip-flop configurations arising for the quadrupole parameter $w_1 \approx 3$ of the neutron star with dominant spin.

We also studied black hole - boson star binaries. In this case, the huge quadrupolar parameter of the boson star allows for significant simplification of the closed subsystem, allowing us to derive a formal analytical solution.

Finally, we analyzed the evolutions of the spin angles numerically by comparing the cases when the black hole companion is either a gravastar, another black hole, or a boson star with identical mass. We found that the amplitude and period of the flip-flop is maximal, when the companion is a black hole. In the case of a boson star companion, the frequency of the flip-flop increased significantly. The precession of the spins is also sensitive to the quadrupolar parameter of the companion. While in the case of gravastars and black holes a swinging-type evolution occurs, when the spins of the components regularly overpass each other, their sequence is conserved when the companion is a boson star.

In a related paper [41] we will discuss the equilibrium of the spin configurations and their linear stability in precessing compact binaries with black hole, neutron star, gravastar, or boson star components.

ACKNOWLEDGMENTS

This work was supported by the Hungarian National Research Development and Innovation Office (NKFIH) in the form of the Grant No. 123996 and has been carried out in the framework of COST actions CA16104 (GWverse) and CA18108 (QG-MM) supported by COST (European Cooperation in Science and Technology). Z. K. was further supported by the János Bolyai Research Scholarship of the Hungarian Academy of Sciences and by the ÚNKP-20-5–New National Excellence Program of the Ministry for Innovation and Technology through its National Research, Development and Innovation Fund. In the early stages of this work, L. Á. G. was supported by the European Union and the State of Hungary, cofinanced by the European Social Fund in the framework of TÁMOP 4.2.4. A/2-11-/1-2012-0001 "National Excellence Program."

APPENDIX: THE PN EXPANSION OF THE RADIAL PERIOD

When averaging instantaneous variables over one radial orbit in order to obtain their secular counterpart, the expression of $\dot{\chi}_p$ given by Eq. (43) of Ref. [59] is needed, as explained in Sec. II A, with both its Newtonian and PN contributions expressible by the true anomaly χ_p and the shape variables $\mathfrak{l}_r(\chi_p)$ and $e_r(\chi_p)$ alone. Hence, $\mathfrak{l}_r(\chi_p)$ and $e_r(\chi_p)$ will be required to 2PN-order accuracy, while the rest of the orbital elements ψ_p, α, and ϕ_n, and spin angles κ_i and ζ_i ($i = 1, 2$) only to leading order, where they are constants.

In this Appendix, first we derive the χ_p dependence of the dimensionless orbital angular momentum $\mathfrak{l}_r$ and the dimensionless orbital eccentricity e_r to 2PN order, in terms of their values at the periastron (characterized by the true anomaly $\chi_p = 0$). Next, employ these expressions to compute the radial period to 2PN accuracy. The derivation of the time-averaged values $\bar{\mathfrak{l}}_r$ and $\bar{e}_r$ over the radial period follows, again to 2PN accuracy, with the inclusion of all spin and mass quadrupole effects to this order. This enables us to express the shape variables evaluated at the periastron in terms of the corresponding averaged quantities. This is

employed for rewriting the radial period as a PN expansion in terms of averaged quantities. At the end of the Appendix, we also give a similar expansion of the averaged PN parameter.

1. χ_p dependence of $\mathfrak{l}_r$

A lower index 0 indicates values taken at $\chi_p = 0$:

$$\mathfrak{l}_r(\chi_p = 0) = \mathfrak{l}_{r0}, \tag{A1}$$

$$e_r(\chi_p = 0) = e_{r0}. \tag{A2}$$

The expressions $\dot{\mathfrak{l}}_r$ and $\dot{\chi}_p$ given by Eqs. (36) and (43) of Ref. [59] allow for deriving

$$\begin{aligned}\mathfrak{l}_r(\chi_p) &= \mathfrak{l}_{r0} + \int_0^{\chi_p} \frac{\dot{\mathfrak{l}}_r}{\dot{\chi}_p} d\chi_p \\ &= \mathfrak{l}_{r0} + \frac{\mathfrak{l}_{rPN}(\chi_p)}{\mathfrak{l}_{r0}} + \frac{\mathfrak{l}_{rSO}(\chi_p)}{\mathfrak{l}_{r0}^2} + \frac{\mathfrak{l}_{rQM}(\chi_p)}{\mathfrak{l}_{r0}^3} \\ &\quad + \frac{\mathfrak{l}_{rSS}(\chi_p)}{\mathfrak{l}_{r0}^3} + \frac{\mathfrak{l}_{r2PN}(\chi_p)}{\mathfrak{l}_{r0}^3},\end{aligned} \tag{A3}$$

with

$$\mathfrak{l}_{rPN}(\chi_p) = 2(2-\eta)e_{r0}(1-\cos\chi_p), \tag{A4}$$

$$\mathfrak{l}_{r2PN}(\chi_p) = \sum_{k=0}^{4}\sum_{l=0}^{2} L_{kl}^{2PN} \sin^{2l}\chi_p \cos^k\chi_p, \tag{A5}$$

$$\begin{aligned}\mathfrak{l}_{rSO}(\chi_p) &= -\frac{\eta e_{r0}}{2}(\cos\chi_p - 1) \\ &\quad \times \sum_{k=1}^{2}(4^{2k-3}+3)\chi_k \cos\kappa_k,\end{aligned} \tag{A6}$$

$$\begin{aligned}\mathfrak{l}_{rSS}(\chi_p) &= \eta\chi_1\chi_2 \sin\kappa_1 \sin\kappa_2 \Bigg[\cos\zeta_+ \sum_{k=0}^{3} L_k^{SS}\cos^k\chi_p \\ &\quad + \sin\zeta_+ \sin\chi_p \sum_{k=0}^{2} K_k^{SS}\cos^k\chi_p\Bigg],\end{aligned} \tag{A7}$$

$$\begin{aligned}\mathfrak{l}_{rQM}(\chi_p) &= \frac{\eta}{2}\sum_{i=1}^{2}\chi_i^2 w_i \nu^{2i-3}\sin^2\kappa_i \Bigg[\cos 2\zeta_i \sum_{k=0}^{3} L_k^{QM}\cos^k\chi_p \\ &\quad + \sin 2\zeta_i \sin\chi_p \sum_{k=0}^{2} K_k^{QM}\cos^k\chi_p\Bigg],\end{aligned} \tag{A8}$$

where the coefficients L_{kl}^{2PN}, L_k^{SS}, K_k^{SS}, L_k^{QM}, and K_k^{QM} are enlisted in Table I.

2. χ_p dependence of e_r

From $\dot{e}_r$ and $\dot{\chi}_p$ given by Eqs. (37) and (43) of Ref. [59], respectively, we find

TABLE I. The coefficients of $\mathfrak{l}_r(\chi_p)$ in Eqs. (A5), (A7), and (A8).

Coefficient	*Expression*
L_{00}^{2PN}	$\frac{1}{96}[432e_{r0}^3\eta + e_{r0}^2(-117\eta^2+54\eta+48)$ $+32e_{r0}(2\eta^2-83\eta+50)$ $-48(\eta^2-5\eta+6)]$
L_{10}^{2PN}	$\frac{e_{r0}}{8}[(2\eta-33)\eta e_{r0}^2$ $-116\eta^2+256\eta-160]$
L_{20}^{2PN}	$\frac{1}{8}[e_{r0}^2(9\eta^2-3\eta-4)$ $+4(\eta^2-5\eta+6)]$
L_{30}^{2PN}	$\frac{e_{r0}}{24}[-3(2\eta+3)\eta e_{r0}^2$ $+32\eta^2-104\eta+80]$
L_{40}^{2PN}	$\frac{3e_{r0}^2(\eta-2)\eta}{32}$
L_{01}^{2PN}	$\frac{1}{8}[e_{r0}^2(-9\eta^2+3\eta+4)$ $-4(\eta^2-5\eta+6)]$
L_{11}^{2PN}	$\frac{e_{r0}}{8}[3(2\eta+3)\eta e_{r0}^2$ $-32\eta^2+104\eta-80]$
L_{21}^{2PN}	$-\frac{9e_{r0}^2(\eta-2)\eta}{16}$
L_{31}^{2PN}	0
L_{41}^{2PN}	0
L_{02}^{2PN}	$\frac{3e_{r0}^2(\eta-2)\eta}{32}$
L_{12}^{2PN}	0
L_{22}^{2PN}	0
L_{32}^{2PN}	0
L_{42}^{2PN}	0
L_0^{SS}	$2e_{r0}+3$
L_1^{SS}	0
L_2^{SS}	-3
L_3^{SS}	$-2e_{r0}$
K_0^{SS}	$-e_{r0}$
K_1^{SS}	-3
K_2^{SS}	$-2e_{r0}$
L_0^{QM}	$-(2e_{r0}+3)$
L_1^{QM}	0
L_2^{QM}	-3
L_3^{QM}	$-2e_{r0}$
K_0^{QM}	$-e_{r0}$
K_1^{QM}	-3
K_2^{QM}	$-2e_{r0}$

$$\begin{aligned}e_r(\chi_p) &= e_{r0} + \int_0^{\chi_p} \frac{\dot{e}_r}{\dot{\chi}_p} d\chi_p \\ &= e_{r0} + \frac{1}{\mathfrak{l}_{r0}^2} e_{rPN}(\chi_p) + \frac{1}{\mathfrak{l}_{r0}^3} e_{rSO}(\chi_p) + \frac{1}{\mathfrak{l}_{r0}^4} e_{rQM}(\chi_p) \\ &\quad + \frac{1}{\mathfrak{l}_{r0}^4} e_{rSS}(\chi_p) + \frac{1}{\mathfrak{l}_{r0}^4} e_{r2PN}(\chi_p),\end{aligned} \tag{A9}$$

with

$$e_{rPN}(\chi_p) = \sum_{k=0}^{3} E_k^{PN} \cos^k \chi_p, \tag{A10}$$

$$e_{rSO}(\chi_p) = \frac{\eta}{2}(1-e_{r0}^2)(1-\cos\chi_p)\sum_{i=1}^{2}(4^{2k-3}+3)\chi_i \cos\kappa_i, \tag{A11}$$

$$e_{r2PN}(\chi_p) = \sum_{l=0}^{3}\sum_{k=0}^{6} E_{kl}^{2PN} \cos^k \chi_p \sin^{2l}\chi_p, \tag{A12}$$

$$e_{rSS}(\chi_p) = \eta\chi_1\chi_2\left[\sum_{k=0}^{5} E_k^{SS}\cos^k\chi_p + \sin\kappa_1\sin\kappa_2\sin\zeta_+\sin\chi_p\sum_{k=0}^{4} F_k^{SS}\cos^k\chi_p\right], \tag{A13}$$

$$e_{rQM}(\chi_p) = \frac{\eta}{2}\sum_{i=1}^{2}\chi_i^2\nu^{2i-3}w_i\left[\sum_{k=0}^{6} E_k^{QM}\cos^k\chi_p + \sin 2\zeta_i \sin^2\kappa_i \sin\chi_p \sum_{k=0}^{4} F_k^{QM}\cos^k\chi_p\right]. \tag{A14}$$

The coefficients E_{kl}^{2PN}, E_k^{SS}, F_k^{SS}, E_k^{QM}, and F_k^{QM} of $e_r(\chi_p)$ for the PN, SS, and QM contributions are collected in Table II. The coefficients E_k^{2PN} and F_k^{2PN} are enlisted in Table III.

TABLE II. The coefficients of $e_r(\chi_p)$ in Eqs. (A10), (A13), and (A14).

Coefficient	*Expression*
E_0^{PN}	$3-\eta+(5-4\eta)e_{r0}+e_{r0}^2(7-6\eta)$
E_1^{PN}	$-[3-\eta+e_{r0}^2(7-\frac{11}{2}\eta)]$
E_2^{PN}	$-(5-4\eta)e_{r0}$
E_3^{PN}	$\frac{\eta}{2}e_{r0}^2$
E_0^{SS}	$-\cos\kappa_1\cos\kappa_2(e_{r0}^2+3e_{r0}+3)$ $+\frac{1}{2}\sin\kappa_1\sin\kappa_2[(e_{r0}^2+3e_{r0}+3)\cos\zeta_-$ $+(7e_{r0}^2+15e_{r0}+5)\cos\zeta_+]$
E_1^{SS}	$\frac{3}{2}\sin\kappa_1\sin\kappa_2(3\cos\zeta_+-\cos\zeta_-)$ $+3\cos\kappa_1\cos\kappa_2$
E_2^{SS}	$\frac{3}{2}e_{r0}\sin\kappa_1\sin\kappa_2(\cos\zeta_+-\cos\zeta_-)$ $+3e_{r0}\cos\kappa_1\cos\kappa_2$
E_3^{SS}	$-\frac{1}{2}e_{r0}^2\sin\kappa_1\sin\kappa_2(\cos\zeta_++\cos\zeta_-)$ $-7\sin\kappa_1\sin\kappa_2\cos\zeta_+$ $+e_{r0}^2\cos\kappa_1\cos\kappa_2$
E_4^{SS}	$-9e_{r0}\sin\kappa_1\sin\kappa_2\cos\zeta_+$
E_5^{SS}	$-3e_{r0}^2\sin\kappa_1\sin\kappa_2\cos\zeta_+$
F_0^{SS}	$1-e_{r0}^2$
F_1^{SS}	$-3e_{r0}$
F_2^{SS}	$-(2e_{r0}^2+7)$
F_3^{SS}	$-9e_{r0}$
F_4^{SS}	$-3e_{r0}^2$
E_0^{QM}	$(7e_{r0}^2+15e_{r0}+5)\cos^2\zeta_i\sin^2\kappa_i$ $+(2e_{r0}^2+3e_{r0}-2)\cos^2\kappa_i$ $-3e_{r0}^2-6e_{r0}-1$
E_1^{QM}	$9\cos^2\kappa_i\sin^2\zeta_i+3(3\cos^2\zeta_i-2)$
E_2^{QM}	$3e_{r0}(2-\cos^2\zeta_i)\cos^2\kappa_i$ $-3e_{r0}\sin^2\zeta_i$
E_3^{QM}	$e_{r0}^2\cos^2\kappa_i$ $+[-(e_{r0}^2+14)\cos^2\zeta_i+7]\sin^2\kappa_i$
E_4^{QM}	$-9e_{r0}\sin^2\kappa_i\cos 2\zeta_i$
E_5^{QM}	$-3e_{r0}^2\sin^2\kappa_i\cos 2\zeta_i$
F_0^{QM}	$(1-e_{r0}^2)$
F_1^{QM}	$-3e_{r0}$
F_2^{QM}	$-(2e_{r0}^2+7)$
F_3^{QM}	$-9e_{r0}$
F_4^{QM}	$-3e_{r0}^2$

3. Dimensionless 2PN orbital period

We insert the expressions of $\mathfrak{l}_r(\chi_p)$ and $e_r(\chi_p)$ into the integral (4) and expand it in Taylor series to 2PN order.

The integral (4) leads to the PN expansion

$$\mathfrak{T} = \mathfrak{T}_0\left(1+\frac{\tau_{0PN}}{\mathfrak{l}_r^2}+\frac{\tau_{0SO}}{\mathfrak{l}_r^3}+\frac{\tau_{0SS}}{\mathfrak{l}_r^4}+\frac{\tau_{0QM}}{\mathfrak{l}_r^4}+\frac{\tau_{02PN}}{\mathfrak{l}_r^4}\right), \tag{A15}$$

where the lower index 0 stands for $\chi_p = 0$. As explained in the main text, $\tau_{0PN}/\mathfrak{l}_r^2$ and $\tau_{02PN}/\mathfrak{l}_r^4$ give PN- and 2PN-order contributions, respectively.

The terms $\mathfrak{T}_0$, τ_{0PN}, τ_{0SO}, τ_{0SS}, τ_{0QM}, and τ_{02PN} are found by exploring the expressions $\mathfrak{l}_r(\chi_p)$ and $e_r(\chi_p)$ derived above. They read as

$$\mathfrak{T}_0 = \frac{2\pi\mathfrak{l}_{r0}^3}{(1-e_{r0}^2)^{3/2}}, \tag{A16}$$

$$\tau_{0PN} = -\frac{(1-e_{r0}^2)(e_{r0}^2(7\eta-6)+2e_{r0}(5\eta-3)+4\eta-18)}{2(e_{r0}-1)^2},$$

$$\tau_{0SO} = 0, \tag{A17}$$

$$\tau_{02PN} = \frac{1}{40(1-e_{r0})^2 e_{r0}^4}\left[\sum_{k=0}^{10} U_k e_{r0}^k - \frac{(1-e_{r0}^2)^{3/2}}{2(1-e_{r0})}\sum_{k=0}^{7} V_k e_{r0}^k\right], \tag{A18}$$

$$\tau_{0SS} = -\frac{3\chi_1\chi_2(1+e_{r0})^2\eta}{(1-e_{r0})\mathfrak{l}_{r0}^4}[\cos\kappa_1\cos\kappa_2+\sin\kappa_1\sin\kappa_2 \times(\sin\zeta_1\sin\zeta_2-2\cos\zeta_1\cos\zeta_2)], \tag{A19}$$

TABLE III. The coefficients of $e_r(\chi_p)$ in Eq. (A12).

Coefficient	Expression
E^{2PN}_{00}	$\frac{1}{1920e_{r0}}[1920e^5_{r0}\eta(3\eta+8)$ $+e^4_{r0}(-1845\eta^2+8880\eta+1800)$ $+32e^3_{r0}(232\eta^2-2825\eta+1740)$ $-180e^2_{r0}(29\eta^2+89\eta+60)$ $+160e_{r0}(8\eta^2-187\eta-60)$ $-480(\eta-3)^2]$
E^{2PN}_{10}	$-\frac{1}{64}[e^4_{r0}\eta(161\eta+477)$ $+4e^2_{r0}(136\eta^2-849\eta+564)$ $+16\eta(8\eta-85)]$
E^{2PN}_{20}	$\frac{1}{256e_{r0}}[e^4_{r0}(269\eta^2-1312\eta-256)$ $+32e^2_{r0}(5\eta^2+109\eta+20)$ $+64(\eta-3)^2]$
E^{2PN}_{30}	$\frac{1}{384}[-3e^4_{r0}\eta(53\eta+73)$ $+8e^2_{r0}(208\eta^2-269\eta+300)$ $+128(4\eta^2-17\eta+15)]$
E^{2PN}_{40}	$\frac{e_{r0}}{128}[e^2_{r0}(-13\eta^2+64\eta+8)$ $+268\eta^2-676\eta+400]$
E^{2PN}_{50}	$-\frac{3e^2_{r0}\eta}{640}[5e^2_{r0}(3\eta-1)-64\eta+80]$
E^{2PN}_{60}	$\frac{3e^3_{r0}\eta^2}{256}$
E^{2PN}_{01}	$-E^{2PN}_{20}$
E^{2PN}_{11}	$-3E^{2PN}_{30}$
E^{2PN}_{21}	$-\frac{3}{2}E^{2PN}_{40}$
E^{2PN}_{31}	$-\frac{1}{10}E^{2PN}_{50}$
E^{2PN}_{41}	$-9E^{2PN}_{60}$
E^{2PN}_{51}	0
E^{2PN}_{61}	0
E^{2PN}_{02}	E^{2PN}_{40}
E^{2PN}_{12}	$\frac{1}{5}E^{2PN}_{50}$
E^{2PN}_{22}	$9E^{2PN}_{60}$
E^{2PN}_{32}	0
E^{2PN}_{42}	0
E^{2PN}_{52}	0
E^{2PN}_{62}	0
E^{2PN}_{03}	$-E^{2PN}_{60}$
E^{2PN}_{13}	0
E^{2PN}_{23}	0
E^{2PN}_{33}	0
E^{2PN}_{43}	0
E^{2PN}_{53}	0
E^{2PN}_{63}	0

$$\tau_{0QM}=-\frac{3\eta(1+e_{r0})^2}{2(1-e_{r0})\mathfrak{l}^4_{r0}}\sum_{i=1}^{2}\chi_i^2\nu^{2i-3}w_i(1-3\sin^2\kappa_i\cos^2\zeta_i). \tag{A20}$$

The coefficients U_k and V_k of τ_{02PN} are enlisted in Table IV.

TABLE IV. The coefficients U_k and V_k of τ_{02PN} in Eq. (A18).

Coefficient	Expression
U_{10}	$-105(\eta+1)\eta$
U_9	$10(-559\eta+297\eta^2+228)$
U_8	$5(-2674\eta+1289\eta^2+1336)$
U_7	$-4(-235\eta+186\eta^2-280)$
U_6	$-482\eta^2+25\eta+1120$
U_5	$2(-17245\eta+5496\eta^2+12200)$
U_4	$2(-2240\eta+79\eta^2+3350)$
U_3	$-4(-7075\eta+2137\eta^2+5300)$
U_2	$2(-3915\eta+1317\eta^2+2050)$
U_1	$40(-254\eta+67\eta^2+210)$
U_0	$-20(-238\eta+65\eta^2+180)$
V_7	$5(-932\eta+509\eta^2+504)$
V_6	$-5(-2700\eta+1399\eta^2+1352)$
V_5	$1427\eta^2+920\eta-4240$
V_4	$12079\eta^2-35880\eta+25680$
V_3	$-4(-6875\eta+2606\eta^2+3650)$
V_2	$-4(-4735\eta+998\eta^2+4850)$
V_1	$40(-746\eta+199\eta^2+600)$
V_0	$-40(-238\eta+65\eta^2+180)$

4. Secular shape variables $\bar{\mathfrak{l}}_r$ and $\bar{e}_r$

Next, we calculate the time averages of the shape variables $\mathfrak{l}_r$ and e_r during one radial period,

$$\bar{\mathfrak{l}}_r=\frac{1}{\mathfrak{T}}\int_0^{2\pi}\frac{\mathfrak{l}_r(\chi_p)}{\dot{\chi}_p}d\chi_p, \tag{A21}$$

$$\bar{e}_r=\frac{1}{\mathfrak{T}}\int_0^{2\pi}\frac{e_r(\chi_p)}{\dot{\chi}_p}d\chi_p, \tag{A22}$$

in terms of their initial values at $\chi_p=0$, with the decomposition of $\mathfrak{T}$ given in Eq. (A15). Their PN expansion can be formally written as

$$\bar{\mathfrak{l}}_r=\frac{\mathfrak{l}_{r0N}+\bar{\mathfrak{l}}_{rPN}+\bar{\mathfrak{l}}_{rSO}+\bar{\mathfrak{l}}_{rSS}+\bar{\mathfrak{l}}_{rQM}+\bar{\mathfrak{l}}_{r2PN}}{\mathfrak{T}}, \tag{A23}$$

$$\bar{e}_r=\frac{e_{r0N}+\bar{e}_{rPN}+\bar{e}_{rSO}+\bar{e}_{rSS}+\bar{e}_{rQM}+\bar{e}_{r2PN}}{\mathfrak{T}}. \tag{A24}$$

The contributions to the integral in Eq. (A21) become

$$\bar{\mathfrak{l}}_{rN}=\frac{2\pi\mathfrak{l}^4_{r0}}{(1-e^2_{r0})^{3/2}}, \tag{A25}$$

$$\bar{\mathfrak{l}}_{rPN}=-\frac{\pi\mathfrak{l}^2_{r0}}{(1-e_{r0})^2\sqrt{1-e^2_{r0}}}[e^2_{r0}(3\eta+2)+14e_{r0}(\eta-1)+4\eta-18], \tag{A26}$$

TABLE V. The coefficients of $\bar{\mathfrak{l}}_r$ in Eqs. (A28) and (A29).

Coefficient	*Expression*
$\bar{L}_4^{2PN}$	$15(467\eta^2-580\eta+296)$
$\bar{L}_3^{2PN}$	$480(4\eta^2-3\eta+5)$
$\bar{L}_2^{2PN}$	$-4(3001\eta^2-9445\eta+6610)$
$\bar{L}_1^{2PN}$	$-480(\eta^2-8\eta+15)$
$\bar{L}_0^{2PN}$	$120(65\eta^2-238\eta+180)$
$\bar{K}_8^{2PN}$	$15\eta(29\eta-3)$
$\bar{K}_7^{2PN}$	$-60(129\eta^2-188\eta+74)$
$\bar{K}_6^{2PN}$	$-15(116\eta^2-711\eta+304)$
$\bar{K}_5^{2PN}$	$2(5516\eta^2-15155\eta+5420)$
$\bar{K}_4^{2PN}$	$-4(5347\eta^2-13720\eta+6400)$
$\bar{K}_3^{2PN}$	$8(\eta^2+2735\eta-4265)$
$\bar{K}_2^{2PN}$	$20308\eta^2-81610\eta+71380$
$\bar{K}_1^{2PN}$	$-720(22\eta^2-82\eta+65)$
$\bar{K}_0^{2PN}$	$60(65\eta^2-238\eta+180)$
$\bar{L}^{SS}$	$4e_{r0}(4e_{r0}^4+29e_{r0}^3+30e_{r0}^2+48e_{r0}+24)$
$\bar{K}^{SS}$	$\cos(\zeta_1+\zeta_2)[96e_{r0}^3-236e_{r0}^2-171e_{r0}^4+95e_{r0}^5+56e_{r0}-32-32\sqrt{1-e_{r0}^2}(e_{r0}^2-e_{r0}^3+e_{r0}-1)]-2e_{r0}\cos(\zeta_1-\zeta_2)(4e_{r0}^4+29e_{r0}^3+30e_{r0}^2+48e_{r0}+24)$

$$\bar{\mathfrak{l}}_{rSO}=-\frac{\pi e_{r0}\eta\mathfrak{l}_{r0}}{(1-e_{r0})\sqrt{1-e_{r0}^2}}\sum_{k=1}^{2}(4^{2k-3}+3)\chi_k\cos\kappa_k, \quad \text{(A27)}$$

$$\bar{\mathfrak{l}}_{r2PN}=\frac{\pi}{120e_{r0}^4}\sum_{k=0}^{4}\bar{L}_k^{2PN}e_{r0}^k-\frac{\pi\sqrt{1-e_{r0}^2}}{60(e_{r0}-1)^4e_{r0}^4}\sum_{k=0}^{8}\bar{K}_k^{2PN}e_{r0}^k, \quad \text{(A28)}$$

$$\bar{\mathfrak{l}}_{rSS}=\frac{\pi\chi_1\chi_2\eta}{16(1-e_{r0})e_{r0}^2(1-e_{r0}^2)^{3/2}}\times(\cos\kappa_1\cos\kappa_2\bar{L}^{SS}+\sin\kappa_1\sin\kappa_2\bar{K}^{SS}), \quad \text{(A29)}$$

$$\bar{\mathfrak{l}}_{rQM}=\frac{\pi(e_{r0}^2+2)\eta}{256e_{r0}(1-e_{r0}^2)^{5/2}}\sum_{k=1}^{2}\chi_k^2\nu^{2k-3}w_k\times[-4(47e_{r0}^3+1050e_{r0}^2+488e_{r0}+480)\sin^2\kappa_k\cos2\zeta_k+16(5e_{r0}^3+21e_{r0}^2+15e_{r0}+6)(3\cos2\kappa_k+1)]. \quad \text{(A30)}$$

The coefficients $\bar{L}_k^{2PN}$, $\bar{K}_k^{2PN}$, $\bar{L}^{SS}$, and $\bar{K}^{SS}$ are collected in Table V.

The integral of Eq. (A22) results in

$$\bar{e}_{rN}=\frac{2\pi e_{r0}\mathfrak{l}_{r0}^3}{(1-e_{r0}^2)^{3/2}}, \quad \text{(A31)}$$

$$\bar{e}_{rPN}=\frac{\pi\mathfrak{l}_{r0}}{e_{r0}}\left\{2(3\eta-5)+\frac{\sqrt{1-e_{r0}^2}}{(1-e_{r0})^3(e_{r0}+1)}[4e_{r0}^4(\eta-2)-20e_{r0}^3(\eta-1)+e_{r0}^2(22-9\eta)+2e_{r0}(5\eta-7)-6\eta+10]\right\}, \quad \text{(A32)}$$

$$\bar{e}_{rSO}=\frac{\pi(e_{r0}+1)\eta}{\sqrt{1-e_{r0}^2}}\sum_{k=1}^{2}(4^{2k-3}+3)\chi_k\cos\kappa_k, \quad \text{(A33)}$$

$$\bar{e}_{r2PN}=\frac{\pi}{480e_{r0}^3\mathfrak{l}_{r0}}\sum_{k=0}^{4}\bar{E}_k^{2PN}e_{r0}^k-\frac{\pi\sqrt{1-e_{r0}^2}}{60(e_{r0}-1)^4e_{r0}^3\mathfrak{l}_{r0}}\sum_{k=0}^{8}\bar{F}_k^{2PN}e_{r0}^k, \quad \text{(A34)}$$

TABLE VI. The coefficients of $\bar{e}_r$ in Eqs. (A34) and (A35).

Coefficient	*Expression*
$\bar{E}_4^{2PN}$	$15(1111\eta^2-1624\eta+528)$
$\bar{E}_3^{2PN}$	$4800(4\eta^2-7\eta+4)$
$\bar{E}_2^{2PN}$	$-4(151\eta^2-7550\eta+5640)$
$\bar{E}_1^{2PN}$	$2880(\eta-3)\eta$
$\bar{E}_0^{2PN}$	$8(1501\eta^2-8090\eta+7260)$
$\bar{F}_8^{2PN}$	$120(\eta-3)\eta$
$\bar{F}_7^{2PN}$	$-60(44\eta^2-107\eta+44)$
$\bar{F}_6^{2PN}$	$-15(317\eta^2-537\eta+96)$
$\bar{F}_5^{2PN}$	$4(457\eta^2-1430\eta-960)$
$\bar{F}_4^{2PN}$	$-5362\eta^2+18335\eta-4380$
$\bar{F}_3^{2PN}$	$-6(714\eta^2-4315\eta+5420)$
$\bar{F}_2^{2PN}$	$21(391\eta^2-2110\eta+2100)$
$\bar{F}_1^{2PN}$	$-4(1411\eta^2-7820\eta+7260)$
$\bar{F}_0^{2PN}$	$1501\eta^2-8090\eta+7260$
$\bar{E}^{SS}$	$16e_{r0}^3(1+e_{r0})^2\sqrt{1-e_{r0}^2}(e_{r0}^2+2)$
$\bar{F}^{SS}$	$-[8(e_{r0}+1)^2\sqrt{1-e_{r0}^2}\times(e_{r0}^2+2)e_{r0}^3\cos(\zeta_1-\zeta_2)+\cos(\zeta_1+\zeta_2)[3176e_{r0}^3-3176e_{r0}^2+1552e_{r0}^4-1552e_{r0}^5-35e_{r0}^6+\sqrt{1-e_{r0}^2}(2376e_{r0}^2-2328e_{r0}^3-468e_{r0}^4+606e_{r0}^5-35e_{r0}^6+92e_{r0}^7+1600e_{r0}-1600)]$

$$\bar{e}_{rSS} = \frac{3\pi\chi_1\chi_2\eta}{16(1-e_{r0})e_{r0}^3(1-e_{r0}^2)^2\mathfrak{l}_{r0}} \times (\cos\kappa_1\cos\kappa_2\bar{E}^{SS} + \sin\kappa_1\sin\kappa_2\bar{F}^{SS}), \quad \text{(A35)}$$

$$\bar{e}_{rQM} = \frac{\pi(e_{r0}^2+2)\eta}{128(1-e_{r0}^2)^{5/2}\mathfrak{l}_{r0}}\sum_{k=1}^{2}\chi_k^2\nu^{2k-3}w_k \times [-4(10e_{r0}^3+609e_{r0}^2+260e_{r0}+336)\sin^2\kappa_k\cos 2\zeta_k + 8(4e_{r0}^3+27e_{r0}^2+15e_{r0}+12)(3\cos 2\kappa_k+1)]. \quad \text{(A36)}$$

The coefficients $\bar{E}_k^{2PN}$, $\bar{F}_k^{2PN}$, $\bar{E}^{SS}$, and $\bar{F}^{SS}$ are collected in Table VI.

5. Initial shape variables in terms of the secular shape variables

The contributions to the averaged shape variables in terms of $\mathfrak{l}_{r0}$ and e_{r0}, Eqs. (A23) and (A24), were presented in the previous subsection. Here, we invert these relations to generate $\mathfrak{l}_{r0}$ and e_{r0} in terms of $\bar{\mathfrak{l}}_r$ and $\bar{e}_r$.

We do this in two steps. First, we take the perturbations to linear order. Using Eqs. (A23), (A25), and (A16) for $\mathfrak{l}_{r0}$, we find

$$\mathfrak{l}_{r0} = \bar{\mathfrak{l}}_r\frac{\mathfrak{T}}{\mathfrak{T}_0} - \frac{1}{\mathfrak{T}_0}(\bar{\mathfrak{l}}_{rPN} + \bar{\mathfrak{l}}_{rSO} + \bar{\mathfrak{l}}_{rSS} + \bar{\mathfrak{l}}_{rQM}). \quad \text{(A37)}$$

Using Eqs (A24), (A31), and (A16), for e_{r0}, we get

$$e_{r0} = \bar{e}_r\frac{\mathfrak{T}}{\mathfrak{T}_0} - \frac{1}{\mathfrak{T}_0}(\bar{e}_{rPN} + \bar{e}_{rSO} + \bar{e}_{rSS} + \bar{e}_{rQM}). \quad \text{(A38)}$$

In the perturbation terms, we can insert the leading-order terms of $\mathfrak{l}_{r0}$ and e_{r0}, which are

$$\mathfrak{l}_{r0} = \bar{\mathfrak{l}}_r, \quad \text{(A39)}$$

$$e_{r0} = \bar{e}_r. \quad \text{(A40)}$$

The results are

$$\mathfrak{l}_{r0PN} = \frac{2\bar{e}_r(\bar{e}_r+1)(\eta-2)}{\bar{\mathfrak{l}}_r}, \quad \text{(A41)}$$

$$\mathfrak{l}_{r0SO} = -\frac{\bar{e}_r(1-\bar{e}_r^2)\eta}{2(\bar{e}_r-1)\bar{\mathfrak{l}}_r^2}\sum_{k=1}^{2}(4^{2k-3}+3)\chi_k\cos\kappa_k, \quad \text{(A42)}$$

$$\mathfrak{l}_{r0SS} = -\frac{\chi_1\chi_2\eta}{32(1-\bar{e}_r)\bar{e}_r^2\bar{\mathfrak{l}}_r^3}(L_0^{SS}\cos\kappa_1\cos\kappa_2 - K_0^{SS}\sin\kappa_1\sin\kappa_2), \quad \text{(A43)}$$

$$\mathfrak{l}_{r0QM} = \frac{\eta}{512\bar{e}_r(\bar{e}_r^2-1)\bar{\mathfrak{l}}_r^3}\sum_{k=1}^{2}\chi_k^2\nu^{2k-3}w_k[-4(47\bar{e}_r^5+1338\bar{e}_r^4+1446\bar{e}_r^3+3444\bar{e}_r^2+1264\bar{e}_r+960) \times\sin^2\kappa_k\cos 2\zeta_k + 16(5\bar{e}_r^5+33\bar{e}_r^4+61\bar{e}_r^3+84\bar{e}_r^2+42\bar{e}_r+12)(3\cos 2\kappa_k+1)], \quad \text{(A44)}$$

where the coefficients L_0^{SS} and K_0^{SS} are listed in Table VII. For e_{r0}, we have

$$e_{r0PN} = \frac{1}{\bar{e}_r\bar{\mathfrak{l}}_r^2}\left\{-(1-\bar{e}_r^2)^{3/2}(3\eta-5) + \frac{(1+\bar{e}_r)^2}{2}[\bar{e}_r^2(11\eta-14) - 2\bar{e}_r(5\eta-7) + 6\eta - 10]\right\}, \quad \text{(A45)}$$

$$e_{r0SO} = -\frac{(\bar{e}_r+1)(1-\bar{e}_r^2)\eta}{2\bar{\mathfrak{l}}_r^3}\sum_{k=1}^{2}(4^{2k-3}+3)\chi_k\cos\kappa_k, \quad \text{(A46)}$$

TABLE VII. The coefficients in Eqs. (A43) and (A51).

Coefficient	*Expression*
$L_{0,2}^{2PN}$	$3(75\eta^2-176\eta+216)$
$L_{0,1}^{2PN}$	$48(3\eta^2-11\eta+10)$
$L_{0,0}^{2PN}$	$86\eta^2-260\eta+176$
$K_{0,4}^{2PN}$	$12(12\eta^2-39\eta+28)$
$K_{0,3}^{2PN}$	$-6(18\eta^2-63\eta+64)$
$K_{0,2}^{2PN}$	$3(17\eta^2-7\eta+28)$
$K_{0,1}^{2PN}$	$-2(7\eta^2+2\eta-32)$
$K_{0,0}^{2PN}$	$43\eta^2-130\eta+88$
L_0^{SS}	$4\bar{e}_r(4\bar{e}_r^4+53\bar{e}_r^3+78\bar{e}_r^2+72\bar{e}_r+24)$
K_0^{SS}	$[-95\bar{e}_r^5+171\bar{e}_r^4-96\bar{e}_r^3+236\bar{e}_r^2-56\bar{e}_r+32-32(1-\bar{e}_r)(1-\bar{e}_r^2)^{3/2}]\times\cos(\zeta_1+\zeta_2)+96\bar{e}_r^2\times(1+\bar{e}_r)^2(2\cos\zeta_1\cos\zeta_2-\sin\zeta_1\sin\zeta_2)+2\bar{e}_r(4\bar{e}_r^4+29\bar{e}_r^3+30\bar{e}_r^2+48\bar{e}_r+24)\times\cos(\zeta_1-\zeta_2)$

$$e_{r0SS} = -\frac{3\chi_1\chi_2\eta}{32(1-\bar{e}_r)\bar{e}_r^3\bar{\mathfrak{l}}_r^4}(E_0^{SS}\cos\kappa_1\cos\kappa_2 - F_0^{SS}\sin\kappa_1\sin\kappa_2), \tag{A47}$$

$$e_{r0QM} = \frac{\eta}{256(\bar{e}_r^2-1)\bar{\mathfrak{l}}_r^4}\sum_{k=1}^{2}\chi_k^2\nu^{2k-3}w_k \times [-4(10\bar{e}_r^5+753\bar{e}_r^4+712\bar{e}_r^3+1986\bar{e}_r^2+664\bar{e}_r+672) \times \sin^2\kappa_k\cos 2\zeta_k + 8(4\bar{e}_r^5+39\bar{e}_r^4+59\bar{e}_r^3+102\bar{e}_r^2+42\bar{e}_r+24)(3\cos 2\kappa_k+1)]. \tag{A48}$$

where the coefficients E_0^{SS} and F_0^{SS} can be found in Table VIII.

The second step is to derive the 2PN terms. For this, we use Eqs. (A23), (A25), and (A16) for $\mathfrak{l}_{r0}$ and Eqs. (A24), (A31), and (A16) for e_{r0}:

$$\mathfrak{l}_{r0} = \bar{\mathfrak{l}}_r\frac{\mathfrak{T}}{\mathfrak{T}_0} - \frac{1}{\mathfrak{T}_0}(\bar{\mathfrak{l}}_{rPN}+\bar{\mathfrak{l}}_{r2PN}), \tag{A49}$$

$$e_{r0} = \bar{e}_r\frac{\mathfrak{T}}{\mathfrak{T}_0} - \frac{1}{\mathfrak{T}_0}(\bar{e}_{rPN}+\bar{e}_{r2PN}). \tag{A50}$$

This time, in order to get the 2PN terms, we need the previously calculated 1PN expressions of $\mathfrak{l}_{r0}$ and e_{r0}. After the Taylor expansion to 2PN order, we find

TABLE VIII. The coefficients in Eqs. (A47) and (A52).

Coefficient	*Expression*
$E_{0,4}^{2PN}$	$15(2915\eta^2-8904\eta+6192)$
$E_{0,3}^{2PN}$	$960(36\eta^2-102\eta+65)$
$E_{0,2}^{2PN}$	$4(7673\eta^2-20110\eta+15360)$
$E_{0,1}^{2PN}$	$960(2\eta^2-11\eta+15)$
$E_{0,0}^{2PN}$	$-8(4559\eta^2-13390\eta+9540)$
$F_{0,6}^{2PN}$	$15(383\eta^2-989\eta+560)$
$F_{0,5}^{2PN}$	$-30(51\eta^2-261\eta+224)$
$F_{0,4}^{2PN}$	$-15(68\eta^2-301\eta+232)$
$F_{0,3}^{2PN}$	$2(893\eta^2-3505\eta+3360)$
$F_{0,2}^{2PN}$	$-2(1756\eta^2-6425\eta+5250)$
$F_{0,1}^{2PN}$	$9358\eta^2-28100\eta+20880$
$F_{0,0}^{2PN}$	$-4559\eta^2+13390\eta-9540$
E_0^{SS}	$16\bar{e}_r^3(1+\bar{e}_r)(\bar{e}_r^3+3\bar{e}_r^2+4\bar{e}_r+2)$
F_0^{SS}	$\cos(\zeta_1+\zeta_2)[92\bar{e}_r^7-35\bar{e}_r^6$ $+606\bar{e}_r^5-468\bar{e}_r^4-2328\bar{e}_r^3$ $+2376\bar{e}_r^2+1600\bar{e}_r-1600$ $+8(\bar{e}_r+1)(3\bar{e}_r^2+200)(1-\bar{e}_r)^{5/2}]$ $+32(\bar{e}_r+1)^2\bar{e}_r^4$ $\times(2\cos\zeta_1\cos\zeta_2-\sin\zeta_1\sin\zeta_2)$ $+8(\bar{e}_r+1)^2(\bar{e}_r^2+2)\bar{e}_r^3$ $\times\cos(\zeta_1-\zeta_2)$

$$\mathfrak{l}_{r02PN} = -\frac{(1-\bar{e}_r^2)^{3/2}}{24\bar{e}_r^2\bar{\mathfrak{l}}_r^3}\sum_{k=0}^{2}L_{0,k}^{2PN}\bar{e}_r^k + \frac{(\bar{e}_r+1)^2}{12\bar{e}_r^2\bar{\mathfrak{l}}_r^3}\sum_{k=0}^{4}K_{0,k}^{2PN}\bar{e}_r^k, \tag{A51}$$

$$e_{r02PN} = -\frac{(1-\bar{e}_r^2)^{3/2}}{960\bar{e}_r^3\bar{\mathfrak{l}}_r^4}\sum_{k=0}^{4}E_{0,k}^{2PN}\bar{e}_r^k + \frac{(1+\bar{e}_r)^2}{120\bar{e}_r^3\bar{\mathfrak{l}}_r^4}\sum_{k=0}^{6}F_{0,k}^{2PN}\bar{e}_r^k. \tag{A52}$$

The coefficients $L_{0,k}^{2PN}$ and $K_{0,k}^{2PN}$ are given in Table VII, while the terms $E_{0,k}^{2PN}$ and $F_{0,k}^{2PN}$ can be found in Table VIII.

The full expressions of $\mathfrak{l}_{r0}$ and e_{r0} are the sum of the corresponding above contributions Eqs. (A39), (A41)–(A44), and (A51) and Eqs. (A40), (A45)–(A48), and (A52), respectively.

6. Radial period in terms of time averages of shape variables

Here, we finally are able to express the radial period in terms of averaged quantities by replacing the initial values at the periastron with time averages over $\chi_p \in [0, 2\pi]$. The various order contributions to Eq. (6) become

$$\tilde{\mathfrak{T}} = \frac{2\bar{\mathfrak{l}}_r^3\pi}{(1-\bar{e}_r^2)^{3/2}}, \tag{A53}$$

$$\tilde{\tau}_{PN} = \sqrt{1-\bar{e}_r^2}(15-9\eta)+(1-\bar{e}_r^2)(7\eta-6), \tag{A54}$$

$$\tilde{\tau}_{SO} = 0, \tag{A55}$$

$$\tilde{\tau}_{2PN} = \frac{\sqrt{1-\bar{e}_r^2}}{64\bar{e}_r^4}\sum_{k=0}^{6}\bar{U}_k\bar{e}_r^k - \frac{(\bar{e}_r+1)}{8\bar{e}_r^4}\sum_{k=0}^{7}\bar{V}_k\bar{e}_r^k, \tag{A56}$$

$$\tilde{\tau}_{QM} = \frac{3\eta}{512\bar{e}_r(1-\bar{e}_r^2)^2}\sum_{k=1}^{2}\chi_k^2\nu^{2k-3}w_k \times [\bar{U}^{QM}\sin^2\kappa_k\cos 2\zeta_k + \bar{V}^{QM}(3\cos 2\kappa_k+1)], \tag{A57}$$

$$\tilde{\tau}_{SS} = \frac{3\chi_1\chi_2\eta}{8(1-\bar{e}_r)^2\bar{e}_r}(\cos\kappa_1\cos\kappa_2\bar{U}^{SS} + \sin\kappa_1\sin\kappa_2\bar{V}^{SS}). \tag{A58}$$

TABLE IX. The coefficients in Eqs. (A56)–(A58).

Coefficient	Expression
$\bar{U}_6$	$-437\eta^2+3336\eta-1008$
$\bar{U}_5$	$-64(8\eta^2-6\eta-5)$
$\bar{U}_4$	$-8(211\eta^2-159\eta+336)$
$\bar{U}_3$	$64(4\eta^2+11\eta-5)$
$\bar{U}_2$	$-8(79\eta^2-600\eta+528)$
$\bar{U}_1$	$-128(\eta^2-8\eta+15)$
$\bar{U}_0$	$32(65\eta^2-238\eta+180)$
$\bar{V}_7$	$224\eta^2-690\eta+360$
$\bar{V}_6$	$2(64\eta^2-11\eta-12)$
$\bar{V}_5$	$139\eta^2-410\eta+452$
$\bar{V}_4$	$-179\eta^2+266\eta-308$
$\bar{V}_3$	$-27\eta^2+28\eta+8$
$\bar{V}_2$	$67\eta^2-4\eta+72$
$\bar{V}_1$	$-12(23\eta^2-90\eta+80)$
$\bar{V}_0$	$260\eta^2-952\eta+720$
$\bar{U}^{QM}$	$-4(27\bar{e}_r^7-72\bar{e}_r^6+263\bar{e}_r^5$ $-1674\bar{e}_r^4-1702\bar{e}_r^3-4116\bar{e}_r^2$ $-1360\bar{e}_r-960)$
$\bar{V}^{QM}$	$16(\bar{e}_r^7-2\bar{e}_r^6+9\bar{e}_r^5-43\bar{e}_r^4$ $-69\bar{e}_r^3-108\bar{e}_r^2-46\bar{e}_r-12)$
$\bar{U}^{SS}$	$-8\bar{e}_r^5+21\bar{e}_r^4-15\bar{e}_r^3$ $-38\bar{e}_r^2-56\bar{e}_r-24$
$\bar{V}^{SS}$	$\frac{\cos(\zeta_1-\zeta_2)}{2}(8\bar{e}_r^5-21\bar{e}_r^4$ $+15\bar{e}_r^3+38\bar{e}_r^2+56\bar{e}_r+24)$ $+\frac{\cos(\zeta_1+\zeta_2)}{4\bar{e}_r^2(\bar{e}_r+1)}[371\bar{e}_r^7-276\bar{e}_r^6$ $+\bar{e}_r^5(-48\bar{e}_r+104\sqrt{1-\bar{e}_r^2}+1771)$ $-\bar{e}_r^4(48\bar{e}_r+104\sqrt{1-\bar{e}_r^2}+1517)$ $+8\bar{e}_r^3(24\bar{e}_r+583\sqrt{1-\bar{e}_r^2}-854)$ $+4\bar{e}_r^2(48\bar{e}_r-1166\sqrt{-\bar{e}_r^2+1}+1881)$ $-8(596\sqrt{1-\bar{e}_r^2}-593)\bar{e}_r$ $+4768(\sqrt{1-\bar{e}_r^2}-1)]$

The coefficients in the above expressions are listed in Table IX.

7. Expansion of the averaged PN parameter

The PN parameter associated to the averaged dynamics is given by

$$\bar{\varepsilon}=\bar{\varepsilon}_{0PN}+\bar{\varepsilon}_{1PN}+\bar{\varepsilon}_{2PN}+\bar{\varepsilon}_{SO}+\bar{\varepsilon}_{SS}+\bar{\varepsilon}_{QM}, \tag{A59}$$

with

$$\bar{\varepsilon}_{0PN}=\frac{2\bar{\mathfrak{l}}_r\pi}{\mathfrak{T}(1-\bar{e}_r^2)^{1/2}}, \tag{A60}$$

$$\bar{\varepsilon}_{1PN}=-\frac{\pi}{\mathfrak{T}\bar{l}_r}[(6-7\eta)(1-\bar{e}_r^2)^{1/2}-9(2-\eta)], \tag{A61}$$

TABLE X. The coefficients M^{SS}, M^{QM}, N^{SS}, and N^{QM} of $\bar{\varepsilon}$ in Eqs. (A63) and (A64).

Coefficient	Expression
M^{SS}	$-2\bar{e}_r+4\bar{e}_r^2-4\bar{e}_r^4+2\bar{e}_r^5$ $-(16\bar{e}_r^2+190+96-19\bar{e}_r^5-203\bar{e}_r^4-110\bar{e}_r^3)\sqrt{1-\bar{e}_r^2}$
N^{SS}	$\cos(\zeta_1+\zeta_2)\{512+2048\bar{e}_r^2$ $-3072\bar{e}_r^4+2048\bar{e}_r^6-512\bar{e}_r^8$ $+[5312-5696\bar{e}_r-1608\bar{e}_r^2$ $+6248\bar{e}_r^3+220\bar{e}_r^4-1994\bar{e}_r^5$ $-5031\bar{e}_r^6+1244\bar{e}_r^7$ $+(-4800+4728\bar{e}_r^2+72\bar{e}_r^4)$ $\times(1-\bar{e}_r)^{3/2}]\sqrt{1-\bar{e}_r^2}\}$ $+8\bar{e}_r(\bar{e}_r+1)\cos(\zeta_1-\zeta_2)$ $[-2\bar{e}_r-4\bar{e}_r^2-4\bar{e}_r^4+2\bar{e}_r^5$ $(-96-190\bar{e}_r-176\bar{e}_r^2-82\bar{e}_r^3$ $+203\bar{e}_r^4+19\bar{e}_r^5)\sqrt{1-\bar{e}_r^2}]$
M^{QM}	$27\bar{e}_r^7-40\bar{e}_r^6+167\bar{e}_r^5-2122\bar{e}_r^4$ $-1990\bar{e}_r^3-3700\bar{e}_r^2-976\bar{e}_r-960$
N^{QM}	$16\bar{e}_r^7+416\bar{e}_r^6+1104\bar{e}_r^5-816\bar{e}_r^4$ $-2064\bar{e}_r^3-2048\bar{e}_r^2-736\bar{e}_r-192$ $+(64\bar{e}_r+64\bar{e}_r^5-128\bar{e}_r^3)\sqrt{1-\bar{e}_r^2}$ $-256(7\bar{e}_r^4+15\bar{e}_r^3-2\bar{e}_r^2$ $-15\bar{e}_r-5)\bar{e}_r^2\sin^2\kappa_i\cos^2\zeta_i$ $+16\{3\bar{e}_r^7-34\bar{e}_r^6-121\bar{e}_r^4-304\bar{e}_r^2$ $-138\bar{e}_r-33\bar{e}_r^5-147\bar{e}_r^3-36$ $+(-24+12\bar{e}_r+12\bar{e}_r^5)\sqrt{1-\bar{e}_r^2}]\cos 2\kappa_i$

$$\bar{\varepsilon}_{SO}=\frac{3\pi}{2\mathfrak{T}\bar{l}_r^2}\left(1-\frac{2}{3}\sqrt{\frac{1+\bar{e}_r}{1-\bar{e}_r}}\right)\sum_{i=1}^{2}\chi_i\cos\kappa_i(4\nu^{2i-3}+3), \tag{A62}$$

$$\bar{\varepsilon}_{SS}=\frac{\pi\chi_1\chi_2\eta}{16\bar{e}_r^2(\bar{e}_r-1)^3(\bar{e}_r+1)^2\bar{\mathfrak{l}}_r^3\mathfrak{T}} \times\{16\bar{e}_r(\bar{e}_r+1)\cos\kappa_1\cos\kappa_2M^{SS}+\sin(\kappa_1)\sin(\kappa_2)N^{SS}\} \tag{A63}$$

$$\bar{\varepsilon}_{QM}=\frac{\pi\eta}{256\bar{e}_r(1-\bar{e}_r^2)^{5/2}\bar{\mathfrak{l}}_r^3\mathfrak{T}}\sum_{i=1}^{2}\nu^{2i-3}\chi_i^2w_i \times\{M^{QM}[\cos(2\kappa_i-2\zeta_i)+\cos(2\kappa_i+2\zeta_i) -2\cos2\zeta_i]+N^{QM}\} \tag{A64}$$

The coefficients of $\bar{\varepsilon}_{SS}$ and $\bar{\varepsilon}_{QM}$ are given in Table X.

$$\bar{\varepsilon}_{2PN}=\frac{-\pi}{4915200(1-\bar{e}_r^2)^{5/2}\bar{e}_r^4\bar{\mathfrak{l}}^3\mathfrak{T}}\{15\bar{e}_r^5M_1^{2PN} -2457600(1+\bar{e}_r)^3\bar{e}_r^3M_2^{2PN}-10240\bar{e}_r^2(1+\bar{e}_r)^2M_3^{2PN} +2(1+\bar{e}_r)[8(1-\bar{e}_r-\bar{e}_r^2+\bar{e}_r^3)\sqrt{1-\bar{e}_r^2} -8+8\bar{e}_r+12\bar{e}_r^2-14\bar{e}_r^3-\bar{e}_r^4]M_4^{2PN} +5[15\bar{e}_r^4-20\bar{e}_r^2-8(1-\bar{e}_r^2)^{5/2}+8]M_5^{2PN}\} \tag{A65}$$

The coefficents of $\bar{\varepsilon}_{2PN}$ are enlisted in Table XI.

TABLE XI. The coefficients M_k^{2PN} of $\bar{\varepsilon}$ in Eq. (A65).

Coefficient	*Expression*
M_1^{2PN}	$-15\eta(98967\eta+118819)\bar{e}_r^6$
	$+1920(\eta(8399\eta-17134)+12016)\bar{e}_r^5$
	$+4(\eta(5837763\eta-15119020)+8076560)\bar{e}_r^4$
	$-5120(\eta(2431\eta-13254)+662)\bar{e}_r^3$
	$+160(41\eta(3071\eta-11629)+502740)\bar{e}_r^2$
	$+40960(\eta(68\eta+1067)-408)\bar{e}_r$
	$+1482240(\eta-3)^2$
M_2^{2PN}	$8(4\eta^2-11\eta+6)\bar{e}_r^5$
	$+(161\eta^2-394\eta+256)\bar{e}_r^4$
	$+(49\eta^2-166\eta+148)\bar{e}_r^3$
	$+2(-25\eta^2+59\eta-48)\bar{e}_r^2$
	$-2(-33\eta^2+83\eta-52)\bar{e}_r$
	$+4(9\eta^2-36\eta+35)$
	$+\sqrt{1-\bar{e}_r^2}[(-12\eta^2+56\eta-64)\bar{e}_r^4$
	$+(24\eta^2-112\eta+128)\bar{e}_r^3$
	$+2(39\eta^2-95\eta+48)\bar{e}_r^2$
	$-2(27\eta^2-51\eta+10)\bar{e}_r$
	$-4(9\eta^2-36\eta+35)]$
M_3^{2PN}	$120(133\eta^2-349\eta+168)\bar{e}_r^8$
	$-240(33\eta^2-155\eta+96)\bar{e}_r^7$
	$+15(-2304\eta^2+5856\eta-3680)\bar{e}_r^6$
	$-2(17\,256\eta^2+37\,520\eta+27\,520)\bar{e}_r^5$
	$+(-14\,856\eta^2+73\,720\eta-47\,360)\bar{e}_r^4$
	$-8(-8312\eta^2+24050\eta-18\,080)\bar{e}_r^3$
	$+4(-6554\eta^2+12260\eta-8720)\bar{e}_r^2$
	$-16(3709\eta^2-11310\eta+8660)\bar{e}_r$
	$+8(3049\eta^2-8490\eta+5660)$
	$+\sqrt{1-\bar{e}_r^2}[15(587\eta^2-2696\eta+1264)$
	$-2(8805\eta^2-40\,440\eta+21\,360)\bar{e}_r^5$
	$+(6177\eta^2-17\,840+27\,280)\bar{e}_r^4$
	$-8(5583\eta^2-12110\eta+12\,280)\bar{e}_r^3$
	$+4(3085\eta^2-1610\eta+360)\bar{e}_r^2$
	$+16(3709\eta^2-11310\eta+8660)\bar{e}_r$
	$-8(3049\eta^2-8490\eta+5660)]$
M_4^{2PN}	$1200\eta(851\eta-3617)\bar{e}_r^6$
	$+15(1731801\eta^2-3339132\eta+1884800)\bar{e}_r^5$
	$+800(37875\eta^2-119180\eta+33904)\bar{e}_r^4$
	$-96(460104\eta^2-1355255\eta+1016100)\bar{e}_r^3$
	$-25600(1177\eta^2+5202\eta-2962)\bar{e}_r^2$
	$-9600(399\eta^2-1814\eta+1851)\bar{e}_r$
	$-153600(43\eta^2-174\eta+135)$
M_5^{2PN}	$15\eta(98967\eta+118819)\bar{e}_r^6$
	$-1920(8399\eta^2-17134\eta+12016)\bar{e}_r^5$
	$-4(5837763\eta^2-15119020\eta+8076560)\bar{e}_r^4$
	$+5120(2431\eta^2-13254\eta+662)\bar{e}_r^3$
	$-160(125911\eta^2-476789\eta+502740)\bar{e}_r^2$
	$-40960(68\eta^2+1067\eta-408)\bar{e}_r$
	$-1482240(\eta-3)^2$

APPENDIX B: REGULAR EVOLUTION DESPITE A JUMP IN $\Delta\zeta$ WHEN ONE OF THE SPINS CROSSES THE ORBITAL ANGULAR MOMENTUM

We note that when either of the spins becomes perpendicular to the orbit Eq. (46) blows up due to the $\sin^{-1}\kappa_i$ and $\cot\kappa_i$ factors, the angle $\Delta\zeta$ becoming ill defined. We show in this subsection that this is but a coordinate singularity.

To illustrate this, we assume that $\sin\kappa_2 \ll 1$, i.e.,

$$\kappa_2(\mathfrak{t}) = \kappa_{(0)2} + \delta\kappa_2(\mathfrak{t}), \tag{B1}$$

with $\kappa_{(0)2} \in \{0,\pi\}$ and $|\delta\kappa_2| \ll 1$. As said before, we are interested in the evolution of $\mathbf{S_2}$ across the orbital angular momentum direction. During this, κ_1 behaves as a quasi-constant (since $\dot{\kappa}_1 \propto \sin\kappa_2$),

$$\kappa_1(\mathfrak{t}) = \kappa_{(0)1} + \delta\kappa_1(\mathfrak{t}), \tag{B2}$$

with $\kappa_{(0)1}$ a constant value and $\delta\kappa_1 \ll 1$. In addition, we assume that $\mathbf{S_1}$ points away from $\mathbf{L_N}$; thus, $\sin\kappa_{(0)1} \gg \cos\kappa_{(0)1}\delta\kappa_1$. Then, the evolution equations for $\Delta\zeta$, $\delta\kappa_1$, and $\delta\kappa_2$ to leading order become

$$\overline{\frac{d\Delta\zeta}{d\mathfrak{t}}} = A_{\Delta\zeta} - B\frac{\cos\Delta\zeta}{\delta\kappa_2}, \tag{B3}$$

$$\overline{\frac{d\delta\kappa_1}{d\mathfrak{t}}} = \epsilon A_{\delta\kappa_1}\delta\kappa_2\sin\Delta\zeta, \tag{B4}$$

$$\overline{\frac{d\delta\kappa_2}{d\mathfrak{t}}} = -B\sin\Delta\zeta, \tag{B5}$$

with $\epsilon = \cos\kappa_{(0)2} = \pm 1$ and the coefficients

$$\frac{A_{\Delta\zeta}}{R} = \nu - \frac{1}{\nu} - \epsilon(2\nu+1)x_2 + (\epsilon+\nu x_2)w_2x_2 + \left(\frac{2}{\nu}+1-w_1-\frac{w_1x_1}{\nu}\cos\kappa_{(0)1}\right)x_1\cos\kappa_{(0)1}, \tag{B6}$$

$$\frac{B}{R} = \left(1+\frac{1}{\nu}-\epsilon x_2-\frac{w_1x_1}{\nu}\cos\kappa_{(0)1}\right)x_1\sin\kappa_{(0)1}, \tag{B7}$$

$$\frac{A_{\delta\kappa_1}}{R} = (1+\nu-\epsilon\nu w_2x_2-x_1\cos\kappa_{(0)1})x_2. \tag{B8}$$

Note that for notational simplicity we omitted the overbar form the secular time derivatives.

From (B3) and (B5), we find

$$\frac{d^2}{d\mathrm{t}^2}[\delta\kappa_2 \sin\Delta\zeta] + A_{\Delta\zeta}^2 \delta\kappa_2 \sin\Delta\zeta = 0, \tag{B9}$$

which gives

$$\delta\kappa_2 \sin\Delta\zeta = Q_1 \cos(A_{\Delta\zeta}\mathrm{t} + G), \tag{B10}$$

with constants $Q_1 > 0$ and G. Then, Eq. (B5) results in

$$(\delta\kappa_2)^2 = -\frac{2BQ_1}{A_{\Delta\zeta}} \sin(A_{\Delta\zeta}\mathrm{t} + G) + Q_2^2, \tag{B11}$$

with an integration constant Q_2^2. By substituting the solutions (B10) and (B11) into Eqs. (B3) and (B5), we find the following relation:

$$Q_2^2 = Q_1^2 + \frac{B^2}{A_{\Delta\zeta}^2}. \tag{B12}$$

With the notation

$$C_1 = \frac{A_{\Delta\zeta}}{B} Q_1, \tag{B13}$$

Eqs. (B10) and (B11) become

$$(\delta\kappa_2)^2 = \frac{B^2}{A_{\Delta\zeta}^2}[1 + C_1^2 - 2C_1 \sin(A_{\Delta\zeta}\mathrm{t} + G)], \tag{B14}$$

$$\sin\Delta\zeta = \frac{BC_1}{A_{\Delta\zeta}} \frac{\cos(A_{\Delta\zeta}\bar{\mathrm{t}} + G)}{\delta\kappa_2}. \tag{B15}$$

The minimum value of $(\delta\kappa_2)^2$ is given by $B^2(1 - C_1)^2/A_{\Delta\zeta}^2$ and when this does not vanish, we find from Eq. (B15) the following restriction for the integration constant C_1:

$$\left(\frac{C_1}{C_1 - 1}\right)^2 < 1. \tag{B16}$$

In the other case when $\delta\kappa_2$ can vanish, the expression (B15) is regular for $\delta\kappa_2 \to 0$ only if $\cos(A_{\Delta\zeta}\bar{\mathrm{t}} + G) \to 0$ at the same time. From Eq. (B14), we find that these conditions can be satisfied only if $\sin(A_{\Delta\zeta}\mathrm{t} + G) \to 1$ for $\delta\kappa_2 \to 0$ and the integration constant C_1 is 1. Then, the solutions read as

$$(\delta\kappa_2)^2 = \frac{2B^2}{A_{\Delta\zeta}^2}[1 - \sin(A_{\Delta\zeta}\mathrm{t} + G)], \tag{B17}$$

$$\sin\Delta\zeta = \frac{B}{A_{\Delta\zeta}} \frac{\cos(A_{\Delta\zeta}\mathrm{t} + G)}{\delta\kappa_2}. \tag{B18}$$

With this expression, from (B4), we have

$$\delta\kappa_1 = \epsilon \frac{A_{\delta\kappa_1} B}{A_{\Delta\zeta}^2} \sin(A_{\Delta\zeta}\mathrm{t} + G) + D, \tag{B19}$$

with D an integration constant.

For $A_{\Delta\zeta}\mathrm{t} + G \to M\pi/2$, where the integer M is chosen such that $\delta\kappa_2 \to 0$ at the same time, we find

$$(\delta\kappa_2)^2 = \frac{B^2}{A_{\Delta\zeta}^2} y^2 \left(1 - \frac{y^2}{12} + \mathcal{O}(y^4)\right), \tag{B20}$$

$$\sin^2\Delta\zeta = 1 - \frac{y^2}{4} + \mathcal{O}(y^4), \tag{B21}$$

with

$$y = A_{\Delta\zeta}\mathrm{t} + G - M\frac{\pi}{2}. \tag{B22}$$

Equations (B20) and (B21) show that, with the exception of the case when κ_1 vanishes but otherwise for general configurations, $\Delta\zeta \to \pm\pi/2$ as $\kappa_2 \to \{0, \pi\}$. According to the definition of polar spin angle, $\delta\kappa_2$ does not change sign when the spin crosses the axis. Thus, from Eq. (B18), we find that $\sin\Delta\zeta$ must change sign as $\delta\kappa_2$ vanishes, implying a jump of $\Delta\zeta$ by π whenever $\mathbf{S}_2$ goes through the axis defined by $\mathbf{L_N}$.

Thus, we have proven that both $\cos\Delta\zeta \propto y$ and $\delta\kappa_2 \propto y$; thus, those terms in Eq. (46) which contain a factor of $\cos\Delta\zeta/\sin\kappa_2$ remain finite as $\sin\kappa_2$ vanishes.

The reverse case, when κ_1 is close to 0 or π but $\sin\kappa_2 \not\approx 0$, can be obtained by interchanging the indices $1 \leftrightarrow 2$ and $\nu \leftrightarrow \nu^{-1}$.

This results shows that the dynamics of the spin angles is well described even if one of $\sin\kappa_i$ evolves through zero.

[1] LIGO Scientific and Virgo Collaborations, GWTC-1: A Gravitational-Wave Transient Catalog of Compact Binary Mergers Observed by LIGO and Virgo during the First and Second Observing Runs, Phys. Rev. X **9**, 031040 (2019).

[2] LIGO Scientific and Virgo Collaborations, GW170817: Observation of Gravitational Waves from a Binary Neutron Star Inspiral, Phys. Rev. Lett. **119**, 161101 (2017).

[3] LIGO Scientific and Virgo Collaborations, GWTC-2: Compact binary coalescences observed by LIGO and Virgo during the first half of the third observing run, arXiv:2010.14527.
[4] C. Kimball, C. P. L. Berry, and V. Kalogera, What GW170729's exceptional mass and spin tells us about its family tree, Res. Notes AAS **4**, 2 (2020).
[5] E. Kun, K. É. Gabányi, M. Karouzos, S. Britzen, and L. Á. Gergely, A spinning supermassive black hole binary model consistent with VLBI observations of the S5 1928 + 738 jet, Mon. Not. R. Astron. Soc. **445**, 1370 (2014).
[6] B. M. Barker and R. F. O'Connell, Derivation of the equations of motion of a gyroscope from the quantum theory of gravitation, Phys. Rev. D **2**, 1428 (1970).
[7] B. M. Barker and R. F. O'Connell, Gravitational two-body problem with arbitrary masses, spins, and quadrupole moments, Phys. Rev. D **12**, 329 (1975).
[8] B. M. Barker and R. F. O'Connell, The gravitational interaction: Spin, rotation, and quantum effects-a review, Gen. Relativ. Gravit. **11**, 149 (1979).
[9] L. E. Kidder, C. M. Will, and A. G. Wiseman, Spin effects in the inspiral of coalescing compact binaries, Phys. Rev. D **47**, R4183 (1993).
[10] L. E. Kidder, Coalescing binary systems of compact objects to $(\text{post})^{5/2}$-Newtonian order. V. Spin effects, Phys. Rev. D **52**, 821 (1995).
[11] C. M. Will, Post-Newtonian gravitational radiation and equations of motion via direct integration of the relaxed Einstein equations. III. Radiation reaction for binary systems with spinning bodies, Phys. Rev. D **71**, 084027 (2005).
[12] H. Wang and C. M. Will, Post-Newtonian gravitational radiation and equations of motion via direct integration of the relaxed Einstein equations. IV. Radiation reaction for binary systems with spin-spin coupling, Phys. Rev. D **75**, 064017 (2007).
[13] P. C. Peters, Gravitational radiation and the motion of two point masses, Phys. Rev. **136**, B1224 (1964).
[14] R. Rieth and G. Schäfer, Spin and tail effects in the gravitational-wave emission of compact binaries, Classical Quant. Grav. **14**, 2357 (1997).
[15] L. Á. Gergely, Z. I. Perjés, and M. Vasúth, Spin effects in gravitational radiation backreaction III. Compact binaries with two spinning components, Phys. Rev. D **58**, 124001 (1998).
[16] L. Á. Gergely, Spin-spin effects in radiating compact binaries, Phys. Rev. D **61**, 024035 (1999).
[17] L. Á. Gergely, Second post-Newtonian radiative evolution of the relative orientations of angular momenta in spinning compact binaries, Phys. Rev. D **62**, 024007 (2000).
[18] A. Klein and P. Jetzer, Spin effects in the phasing of gravitational waves from binaries on eccentric orbits, Phys. Rev. D **81**, 124001 (2010).
[19] E. Poisson, Gravitational waves from inspiraling compact binaries: The quadrupole-moment term, Phys. Rev. D **57**, 5287 (1998).
[20] L. Á. Gergely and Z. Keresztes, Gravitational radiation reaction in compact binary systems: Contribution of the quadrupole-monopole interaction, Phys. Rev. D **67**, 024020 (2003).
[21] É. Racine, Analysis of spin precession in binary black hole systems including quadrupole-monopole interaction, Phys. Rev. D **78**, 044021 (2008).
[22] T. Hinderer, B. D. Lackey, R. N. Lang, and J. S. Read, Tidal deformability of neutron stars with realistic equations of state and their gravitational wave signatures in binary inspiral, Phys. Rev. D **81**, 123016 (2010).
[23] J. Vines, É. É. Flanagan, and T. Hinderer, Post-1-Newtonian tidal effects in the gravitational waveform from binary inspirals, Phys. Rev. D **83**, 084051 (2011).
[24] A. Buonanno, G. Faye, and T. Hinderer, Spin effects on gravitational waves from inspiraling compact binaries at second post-Newtonian order, Phys. Rev. D **87**, 044009 (2013).
[25] B. Mikóczi, M. Vasúth, and L. Á. Gergely, Self-interaction spin effects in inspiralling compact binaries, Phys. Rev. D **71**, 124043 (2005).
[26] T. Marchand, L. Bernard, L. Blanchet, and G. Faye, Ambiguity-free completion of the equations of motion of compact binary systems at the fourth post-Newtonian order, Phys. Rev. D **97**, 044023 (2018).
[27] L. Bernard, L. Blanchet, G. Faye, and T. Marchand, Center-of-mass equations of motion and conserved integrals of compact binary systems at the fourth post-Newtonian order, Phys. Rev. D **97**, 044037 (2018).
[28] M. Levi and J. Steinhoff, Complete conservative dynamics for inspiralling compact binaries with spins at fourth post-Newtonian order, arXiv:1607.04252.
[29] G. Schäfer and P. Jaranowski, Hamiltonian formulation of general relativity and post-Newtonian dynamics of compact binaries, Living Rev. Relativity **21**, 7 (2018).
[30] T. A. Apostolatos, C. Cutler, G. J. Sussman, and K. S. Thorne, Spin-induced orbital precession and its modulation of the gravitational waveforms from merging binaries, Phys. Rev. D **49**, 6274 (1994).
[31] L. Á. Gergely and P. L. Biermann, The spin-flip phenomenon in supermassive black hole binary mergers, Astrophys. J. **697**, 1621 (2009).
[32] Gopal-Krishna, P. L. Biermann, L. Á. Gergely, and P. J. Wiita, On the origin of x-shaped radio galaxies, Res. Astron. Astrophys. **12**, 127 (2012).
[33] M. Kesden, D. Gerosa, R. O'Shaughnessy, E. Berti, and U. Sperhake, Effective Potentials and Morphological Transitions for Binary Black-Hole Spin Precession, Phys. Rev. Lett. **114**, 081103 (2015).
[34] D. Gerosa, M. Kesden, U. Sperhake, E. Berti, and R. O'Shaughnessy, Multi-timescale analysis of phase transitions in precessing black-hole binaries, Phys. Rev. D **92**, 064016 (2015).
[35] C. O. Lousto and J. Healy, Flip-Flopping Binary Black Holes, Phys. Rev. Lett. **114**, 141101 (2015).
[36] C. O. Lousto and J. Healy, Unstable flip-flopping spinning binary black holes, Phys. Rev. D **93**, 124074 (2016).
[37] C. O. Lousto, J. Healy, and H. Nakano, Spin flips in generic black hole binaries, Phys. Rev. D **93**, 044031 (2016).
[38] J. Majár, Spin-spin interaction in the spin-precession equations, Phys. Rev. D **80**, 104028 (2009).
[39] D. Gerosa, A. Lima, E. Berti, U. Sperhake, M. Kesden, and R. O'Shaughnessy, Wide nutation: Binary black-hole spins

repeatedly oscillating from full alignment to full anti-alignment, Classical Quant. Grav. **36**, 105003 (2019).
[40] M. Kesden, D. Gerosa, R. O'Shaughnessy, E. Berti, and U. Sperhake, Effective Potentials and Morphological Transitions for Binary Black Hole Spin Precession, Phys. Rev. Lett. **114**, 081103 (2015).
[41] LIGO Scientific and Virgo Collaborations, GW190425: Observation of a compact binary coalescence with total mass $\sim 3.4 M_{\odot}$, Astrophys. J. Lett. **892**, L3 (2020).
[42] D. Radice, A. Perego, F. Zappa, and S. Bernuzzi, GW170817: Joint constraint on the neutron star equation of state from multimessenger observations, Astrophys. J. Lett. **852**, L29 (2018).
[43] W. G. Laarakkers and E. Poisson, Quadrupole Moments of rotating neutron stars, Astrophys. J. **512**, 282 (1999).
[44] M. Urbanec, J. C. Miller, and Z. Stuchlik, Quadrupole moments of rotating neutron stars and strange stars, Mon. Not. R. Astron. Soc. **433**, 1903 (2013).
[45] F. D. Ryan, Spinning boson stars with large self-interaction, Phys. Rev. D **55**, 6081 (1997).
[46] N. Uchikata, S. Yoshida, and P. Pani, Tidal deformability and I-Love-Q relations for gravastars with polytropic thin shells, Phys. Rev. D **94**, 064015 (2016).
[47] R. M. O'Leary, B. Kocsis, and A. Loeb, Gravitational waves from scattering of stellar-mass black holes in galactic nuclei, Mon. Not. R. Astron. Soc. **395**, 2127 (2009).
[48] B. Kocsis and J. Levin, Repeated bursts from relativistic scattering of compact objects in galactic nuclei, Phys. Rev. D **85**, 123005 (2012).
[49] J. Cuadra, P. J. Armitage, R. D. Alexander, and M. C. Begelman, Massive black hole binary mergers within subparsec scale gas discs, Mon. Not. R. Astron. Soc. **393**, 1423 (2009).
[50] A. Sesana, Self consistent model for the evolution of eccentric massive black hole binaries in stellar environments: Implications for gravitational wave observations, Astrophys. J. **719**, 851 (2010).
[51] L. Wen, On the eccentricity distribution of coalescing black hole binaries driven by the Kozai mechanism in globular clusters, Astrophys. J. **598**, 419 (2003).
[52] L. Hoffman and L. Loeb, Dynamics of triple black hole systems in hierarchically merging massive galaxies, Mon. Not. R. Astron. Soc. **377**, 957 (2007).
[53] N. Seto, Relativistic resonant relations between massive black hole binary and extreme mass ratio inspiral, Phys. Rev. D **85**, 064037 (2012).
[54] S. Naoz, B. Kocsis, A. Loeb, and N. Yunes, Resonant post-Newtonian eccentricity excitation in hierarchical three-body systems, Astrophys. J. **773**, 187 (2013).
[55] M. Preto, I. Berentzen, P. Berczik, D. Merritt, and R. Spurzem, Merger of massive black holes using N-body simulations with post-Newtonian corrections, J. Phys. Conf. Ser. **154**, 012049 (2009).
[56] U. Löckmann and H. Baumgardt, Tracing intermediate-mass black holes in the Galactic Centre, Mon. Not. R. Astron. Soc. **384**, 323 (2008).
[57] L. Á. Gergely, Spinning compact binary inspiral: Independent variables and dynamically preserved spin configurations, Phys. Rev. D **81**, 084025 (2010).
[58] L. Á. Gergely, Spinning compact binary inspiral. II. Conservative angular dynamics, Phys. Rev. D **82**, 104031 (2010).
[59] L. Á. Gergely and Z. Keresztes, Spinning compact binary dynamics and chameleon orbits, Phys. Rev. D **91**, 024012 (2015).
[60] T. Damour and N. Deruelle, General relativistic celestial mechanics of binary systems. I. The post-Newtonian motion, Ann. Inst. Henri Poincaré (Phys. Théor.) **43**, 107 (1985).
[61] L. Blanchet, Gravitational radiation from post-Newtonian sources and inspiralling compact binaries, Living Rev. Relativity **17**, 2 (2014).
[62] S. Ossokine, M. Boyle, L. E. Kidder, H. P. Pfeiffer, M. A. Scheel, and B. Szilágyi, Comparing post-Newtonian and numerical-relativity precession dynamics, Phys. Rev. D **92**, 104028 (2015).
[63] Z. Keresztes, B. Mikóczi, and L. Á. Gergely, Kepler equation for inspiralling compact binaries, Phys. Rev. D **72**, 104022 (2005).
[64] B. Mikóczi, Spin supplementary conditions for spinning compact binaries, Phys. Rev. D **95**, 064023 (2017).
[65] T. D. Newton and E. P. Wigner, Localized states for elementary systems, Rev. Mod. Phys. **21**, 400 (1949).
[66] M. H. L. Pryce, The mass center in the restricted theory of relativity and its connection with the quantum theory of elementary particles, Proc. R. Soc. A **195**, 62 (1948).
[67] J. Vinti, D. Ger, and A. Bonavito, *Orbital and Celestial Mechanics* (American Institute of Aeronautics and Astronautics, Reston, VA, 1998), Vol. 177.
[68] N. Warburton, T. Osburn, and C. R. Evans, Evolution of small-mass-ratio binaries with a spinning secondary, Phys. Rev. D **96**, 084057 (2017).
[69] Z. Keresztes and L. Á. Gergely, following paper, Stability analysis of the spin evolution fix points in inspiraling compact binaries with black hole, neutron star, gravastar or boson star components, Phys. Rev. D **103**, 084025 (2021).